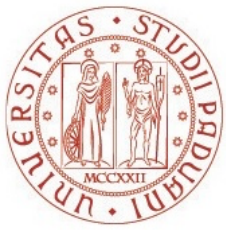

UNIVERSITÀ DEGLI STUDI DI PADOVA
Department of Land, Environment Agriculture and Forestry

Second Cycle Degree (MSc)
in Forest Science

Innovative application of xylem anatomy to investigate the complex relationships between carbon sequestration and biomass growth in a Norway spruce forest in the Italian Alps

Supervisor
Prof. Daniele Castagneri

Submitted by:
Emeka Vitalis Nwonu
Student no. 2047601

ACADEMIC YEAR
2021-2022

Table of Contents

List of Tables

List of Figures

Abbreviations and acronyms

GPP	Gross primary productivity
NEP	Net ecosystem productivity
NEE	Net ecosystem exchange
GEP	Gross ecosystem productivity
RECO	Ecosystem respiration
ICOS	Integrated carbon observation systems
EC	Eddy covariance
VUT	Variable USTAR threshold
CUT	Constant USTAR threshold
ROXAS	Root xylem analysis system
CWA	Cell wall area
NUM	Cell number
EW	Earlywood
LW	Latewood
NSC	Non-structural carbohydrate

Acknowledgement

I want to specially thank my Supervisor, Professor Daniele Castagneri, TESAF Department, University of Padova (UNIPD), for his unfathomable wealth of wisdom, knowledge and encouragement. His expertise, professionalism and open-door policy guided me throughout the thesis period and has chatted a new course for me. I am ever grateful.

To all my Professors at UNIPD, especially Professors Lorenzo Picco, Vincenzo D'Agostino, and Paola Gatto for their immense intellectual contributions towards the success of my master's program. Also, to all my University of Copenhagen (UCPH) Professors- most especially Niels Strange, Karsten Raulund-Rasmussen and Iben Nathan for their dedication and commitment.

A very big thank you to Dr. Paulina Puchi, Postdoctoral Fellow, TESAF, UNIPD, Dr. Genny Fanchin, the Technician TESAF, UNIPD and Mr. Johannes De Koning, PhD student at UCPH for their support and immeasurable contribution towards this thesis and my academic success.

Permit me to thank all SUFONAMA, other Erasmus Mundus Scholars, regular forestry students at UCPH and UNIPD, and an inumerable international students from across the globe, for their mutual understanding. The two years in Europe has enriched my cultural, political and religious understanding, through interactions with fellow students and residence mates from Albania, Armenia, Bangladesh, Brazil, Cameroon, Canada, Chile, China, Colombia, Czech, Denmark, Egypt, Ethiopia, Faroe Island, Finland, France, Germany, Ghana, India, Italy, Kazakhstan, Lebanon, Nepal, Niger, Pakistan, Palestine, Poland, Romania, Russia, South Korea, Spain, Sudan, Tunisia, Ukraine, United Kingdom, Vietnam and Zimbabwe. A big thank you too to Desalegn Yadeta from Ethiopia and my compatriots, Magnus Onyiriagwu and Dosumu Babatunde for the shared time and brotherliness these two years.

To the European Union for the financial support which enable me to effectively participate in the Erasmus Mundus Joint Master's Degree program.

Above all, my biggest thanks to the Almighty God for the gifts of life, supporting family members, dedicated Professors and wonderful friends. To God be all the glory.

Dedication

I dedicate my double master's degree Certificates from UCPH and UNIPD to my late mother, Mrs. Janeth Nwafor Nwonu who transitioned to eternal glory during my studies. Your legacies speak volume ma. Rest on till we meet on the resurrection morning.

ABSTRACT

The forest ecosystems are one of the main global carbon sinks, sequestering about 30% of total anthropogenic CO_2. Due to uncertainties and interannual variabilities in the estimation of forest carbon balance, several studies found an inconsistent link between tree biomass increment and ecosystem primary productivity measured by eddy covariance. This thesis innovatively investigated the complex relationship between the forest carbon flux and the tree biomass using quantitative wood anatomy. In the Norway spruce forest of Renon, Italian Alps, the intra-annual variabilities of xylem anatomical features of Norway spruce were correlated with eddy covariance data. Seven trees were selected for the anatomy analysis which spanned from 1934 to 2020. Two xylem anatomical traits, the cell wall area (CWA), and the cell number (NUM) were analyzed. The results showed that the CWA in earlywood responded positively to winter precipitation while CWA in latewood (LW) and cell number in earlywood (EW) and latewood were influenced by temperature. The CWA in earlywood and latewood yielded negative and mostly non-significant correlation with the eddy covariance gross primary productivity (GPP) while a marginal positive correlation, was obtained for NUM_EW and NUM_LW with GPP. This study evidences climate influence on gross primary productivity (GPP), particularly in early spring when temperatures are generally above 0 at the site. Furthermore, May-September temperature correlation with CWA in latewood indicates that carbon sink at the end of the growing season was affected by climate. However, low associations between anatomical traits and GPP were observed. The incompatibility could be attributed to the absence of reliable techniques to measure advective fluxes on sloping terrains and the storage of photosynthates in non-structural carbohydrate pools. The negative correlation between CWA in earlywood and latewood with spring and summer GPP respectively, suggests that photosynthates were not immediately mobilized for stem growth and this calls for further research on an integrated quantification of other carbon storage pools for closure in forest carbon balance.

Keywords: Dendroanatomy, quantitative wood anatomy, gross primary productivity, tree biomass, ROXAS, xylem anatomical traits.

RIASSUNTO

Gli ecosistemi forestali sono uno dei principali serbatoi di carbonio a livello globale, in quanto sequestrano circa il 30% della CO2 antropogenica totale. A causa delle incertezze e delle variabilità interannuali nella stima del bilancio del carbonio forestale, diversi studi hanno riscontrato un legame incoerente tra l'incremento della biomassa arborea e la produttività primaria dell'ecosistema misurata mediante eddy covariance. Questa tesi ha indagato in modo innovativo la complessa relazione tra il flusso di carbonio della foresta e la biomassa degli alberi utilizzando l'anatomia quantitativa del legno. Nella foresta di abete rosso del Renon, nelle Alpi italiane, le variabilità intra-annuali delle caratteristiche anatomiche dello xilema dell'abete rosso sono state correlate con i dati di eddy covariance. Sono stati selezionati sette alberi per l'analisi dell'anatomia, che ha spaziato dal 1934 al 2020. Sono stati analizzati due tratti anatomici dello xilema, l'area della parete cellulare (CWA) e il numero di cellule (NUM). I risultati hanno mostrato che il CWA nel legno primaticcio ha risposto positivamente alle precipitazioni invernali, mentre il CWA nel legno tardivo (LW) e il numero di cellule nel legno primaticcio (EW) e nel legno tardivo sono stati influenzati dalla temperatura. Il CWA nell'earlywood e nel latewood ha prodotto una correlazione negativa e per lo più non significativa con la produttività primaria lorda (GPP) eddy covariance, mentre una correlazione positiva marginale è stata ottenuta per NUM_EW e NUM_LW con la GPP. Questo studio evidenzia l'influenza del clima sulla produttività primaria (GPP), in particolare all'inizio della primavera, quando le temperature sono generalmente superiori a 0 nel sito. Inoltre, la correlazione tra la temperatura di maggio-settembre e il CWA nel legno tardivo indica che l'assorbimento di carbonio alla fine della stagione di crescita è influenzato dal clima. Tuttavia, sono state osservate basse associazioni tra i tratti anatomici e la GPP. L'incompatibilità potrebbe essere attribuita all'assenza di tecniche affidabili per misurare i flussi advettivi su terreni in pendenza e all'immagazzinamento dei fotosintati in pool di carboidrati non strutturali. La correlazione negativa tra il CWA nel legno primaticcio e nel legno tardivo con la GPP primaverile ed estiva, rispettivamente, suggerisce che i fotosintati non sono stati immediatamente mobilitati per la crescita del fusto e ciò richiede ulteriori ricerche sulla quantificazione integrata di altri pool di stoccaggio del carbonio per la chiusura del bilancio del carbonio della foresta.

Parole chiave: Dendroanatomia, anatomia quantitativa del legno, produttività primaria lorda, biomassa arborea, ROXAS, tratti anatomici dello xilema.

1. INTRODUCTION

Terrestrial ecosystems dominated by forests, grasslands, shrublands, croplands, and savanna, absorb about 112-169 PgC each year from the atmosphere through the anabolic mechanism of photosynthesis (Sha et al., 2022). Narrowing it down, the global forests, recognized as an essential terrestrial carbon sink (Teets et al., 2018), sequester roughly 30% of the total anthropogenic CO_2 emissions (Alexander et al., 2018; Aubinet et al., 2018; Babst et al., 2014a). This implies that if promoted, the forest ecosystem productivity could be a rallying point for climate change mitigation and adaptation. However, this capacity of the forest to store CO_2 from the atmosphere is threatened by the saturation effect and harsh environmental conditions (Anić et al., 2018). The estimates of the captured carbon in the forest vary from year to year, and the mechanism of the utilization or allocation of carbon to long-term pools like woody biomass is still poorly understood, thereby making it difficult to predict the future forest carbon balance (Aubinet et al., 2018; Babst et al., 2014b). To this end, research must reduce the uncertainties in estimates of the carbon allocation to forest biomass (Babst et al., 2014b).

1.1 Eddy Covariance Techniques

In recent decades, research efforts were intensified to unravel the mechanism and the main drivers of carbon sequestration in the forest with the adoption of the eddy covariance (EC) technique which is a method to measure, in a direct and defensible manner, the vertical turbulent fluxes of momentum, energy, and gases between the atmosphere and the ecosystems (Babst et al., 2014b; Rannik et al., 2020). In the forest ecosystem, EC measures the forest-atmosphere gas (including water and CO_2) and energy exchanges (Baldocchi et al., 2018; Baldocchi, 2003; Tramontana et al., 2020). With the introduction of the EC techniques in the late ’90s, it is currently feasible to measure the seasonal fluxes over tall vegetations (Babst et al., 2014b). This micrometeorological method measures the net carbon dioxide (CO_2) exchange at a high frequency (usually 10Hz) by estimating the covariance between fluctuations in vertical wind velocity and the CO_2 mixing ratio in the ecosystem (Jia et al., 2022).

One of the overarching goals of the EC flux networks is to garner time-series data that can assess the biophysical factors affecting interannual variability and/or detect temporal trends in the carbon fluxes (Baldocchi et al., 2018). The carbon which enters the ecosystem through photosynthesis results in gross primary production (GPP): part of the carbon is used for autotrophic respiration (Ra). The difference between the GPP and the Ra gives the net primary

production (NPP). Heterotrophic respiration (Rh) from heterotrophic organisms in the ecosystem causes a net carbon loss. Consequently, the sum of the Ra and Rh results in the ecosystem respiration (Reco). The net ecosystem productivity (NEP) is given as the negative value of the net ecosystem exchange (NEE). This implies that NEP = (-NEE) = GPP-Reco or NPP-Rh (Anić et al., 2018; Baldocchi et al., 2018; Papale et al., 2015; Zanotelli et al., 2015). The NEP shows if an ecosystem is a carbon sink (when positive) or carbon source (when negative) (Zanotelli et al., 2015).

To unify the data processing protocol and establish a global database of EC, a global FLUXNET network has been created to receive different ecosystems data from EC sites, organized in regional networks such as integrated carbon observation systems (ICOS), AmeriFlux, and AsiaFlux. Forest EC sites mostly have records of less than 10 years (Pastorello, 2020).

Though Ecologists, who focus on the temporal variations in forest net primary production and Dendrochronologists, who study, albeit retrospectively, the relationship between tree-ring width and the climate variability, have one thing in common - the understanding of the relationship between climate variability and plant growth, only a few studies worldwide have used tree-ring width analyses to assess the above-ground growth of trees in the flux track of EC towers to illuminate the relationships between net ecosystem production (NEP), gross ecosystem production (GEP), and aboveground biomass accumulation (above ground volume) (Aubinet et al., 2018; Babst et al., 2018; Pastorello, 2020; Rocha et al., 2006; Teets et al., 2018). Ring width analyses allow the assessment of growth variability over the entire tree lifespan, which can be much longer than the period covered by forest inventories (Pappas et al., 2020). Moreover, tree rings provide an annual resolution, which is not the case for most inventories. Using allometric equations, tree volume increment can be derived from tree-ring patterns. The aboveground biomass can be calculated from the volume and wood density (Babst et al., 2014b; Pappas et al., 2020). Finally, the aboveground carbon stock can be inferred from tree biomass considering the wood carbon content.

1.2 Tree rings and forest woody biomass

Tree rings studies have been widely employed in forest research to get estimates of forest woody production. Besides tree rings, field plot measurement (González-García et al., 2016; Peng et al., 2009; Xu et al., 2019) has being used to model forest wood biomass increment;

however, tree rings offer a higher temporal and spatial resolution as they allow the reconstruction of historical annual (and intra-annual) woody biomass increment over long periods (Babst et al., 2014a; Xu et al., 2019). Besides total ring width, other tree ring measurements include A) Earlywood and latewood, width. B) Wood density – earlywood, latewood, minimum and maximum density. C) Stable isotope ratios - carbon, nitrogen, oxygen, hydrogen. D) Blue light reflected from the wood surface. E) The abundance of a particular chemical compound. F) Wood anatomical features – cell number, size, cell lumen area, cell wall area and thickness. (Babst et al., 2014a; Berger et al., 2004; Campbell et al., 2007). The analysis of the latter group is called dendroanatomy, which is the application of quantitative wood anatomy along tree ring series. This approach highlights the variability in xylem anatomical traits of shrubs, trees, and herbaceous plants to understand their structure, function, growth, and environmental intricacies (von Arx et al., 2016). The functions of the xylem in plants are wide-ranging to ensure their survival and growth. The xylem allows the transport of water, sugars, hormones, buffer water flow, and nutrients. It equally supports the mass of the canopy among other functions (Castagneri et al., 2017; von Arx et al., 2016). The wood formation known as xylogenesis is highly influenced by the prevailing environmental conditions (Cuny et al., 2015); thus, xylem anatomical features have become a natural archive to study the plant growth-environmental relationship and plant functioning with intra-annual resolution (Fonti et al., 2010; von Arx et al., 2016).

1.3 Research Gap

Co-located study of GPP and tree growth is crucial to cross-match the ecosystem carbon uptake and tree biomass increment (Cabon et al., 2022). Previous studies have found an inconsistent link between tree biomass increment and the GPP measured with EC (Babst et al., 2013; Delpierre et al., 2016; Rocha et al., 2006; Teets et al., 2018; Zweifel et al., 2010). While Babst et al. (2013) and Teets et al. (2018) found a positive correlation, Delpierre et al. (2016) found a negative correlation. The inconsistency were attributed to differential increment in living and non-living carbon stocks (Delpierre et al., 2016) and the presence of non-photosynthetic factors controlling tree growth (Cabon et al., 2022; Rocha et al., 2006). So far, no research has employed the technique of xylem anatomy, which analyzes the building blocks of woody biomass, at intra annual level, to investigate the link between aboveground woody biomass and EC.

1.4 Objectives

The general objective of the study is to investigate the link between forest carbon atmospheric uptake (carbon fluxes) and woody biomass increment using xylem anatomical traits. Specific objectives were:

1. To assess the relationships between different components of xylem biomass, i.e., the number of tracheids and cell wall area, in earlywood and latewood.
2. To assess the influence of climate variability on the primary productivity (GPP) and xylem biomass proxies.
3. To evaluate the relationship between the tree-ring biomass proxies and the GPP.

1.5 Hypotheses

1. Xylem anatomical features are related to carbon fluxes (GPP from EC): Assuming that at least some carbon taken during photosynthesis was rapidly mobilized for cell growth, the xylem earlywood biomass would correlate with the spring GPP while xylem latewood biomass with the late summer GPP.

2. Climatic influence on the carbon fluxes and tree growth is synchronous: Assuming that temperature and precipitation influence carbon sequestration and xylem biomass proxies, a mutually non-exclusive climatic relationship would be obtained for GPP and tree biomass increment.

2. MATERIALS AND METHOD

2.1 Study area

Renon forest is a sub-alpine coniferous forest located in the Italian Alps (46.58° N, 11.43 E, 1735 m a.s.l.). The stand is equipped with an eddy covariance (EC) tower (Figure 1) installed in 1997, making it one of the oldest EC sites in Italy. The forest is uneven-aged with the oldest trees being about 200 years old. The soil is classified as Haplic podsol according to FAO (Papale et al., 2015). The main tree species in the forest are Norway spruce (*Picea abies* (L.) Karst.), comprising of 85% of all the trees, others are cembran pine (*Pinus cembra* L.) covering 12% and larch (*Larix decidua* Mill.), making up the remaining 3% (Montagnani et al., 2009). The climate is affected strongly by elevation with cool summers and moderately cold winters. The annual mean temperature and the annual mean precipitation are 6.2 ºC and 964 mm, respectively (Niu et al., 2011). Climate and environmental monitoring and studies on carbon fluxes (Table 1) have been carried out in recent years (Montagnani et al., 2009; Niu et al., 2011; Papale et al., 2015).

Figure 1: Eddy covariance tower at Renon forest.

Table 1: Site properties of Renon forest.

Site properties	Value	Source
Longitude, latitude	11°17' E, 46°25' N	
Elevation (m)	1735	
Major species	Norway spruce (*Picea abies*)	
Canopy height (m)	29-31	(Marcolla et al., 2005; Montagnani et al., 2009)
Topography	Alpine slope (11°)	(Feigenwinter et al., 2008)
LAI (m^2 m^{-2})	5.1-5.5	(Marcolla et al., 2005; Montagnani et al., 2009)
Annual NEE (g C m^{-2})	-450	(Feigenwinter et al., 2008; Montagnani et al., 2009)
Stand age	Uneven	(Feigenwinter et al., 2008)
Average stems per hectare	270	(Marcolla et al., 2005)
Annual mean temperature (°C)	6.21	(Niu et al., 2011)
Annual mean precipitation (mm)	964.21	(Niu et al., 2011)
Height of EC mast (m)	42	(Marcolla et al., 2005)

2.2 Sample collection and preparation

In summer 2021, from the EC tower footprint, 20 trees were cored using an increment borer of 5 mm of diameter at 1.3 m from ground level. In the laboratory, all cores were sanded with increasingly finer sandpaper to evidence tree ring boundaries. Then, ring widths were measured to the nearest 0.01 mm using TsapWin (Rinntech, Heidelberg, Germany) associated to LINTAB table. The samples were visually and statistically cross-dated to ensure a match between tree rings and their actual year of formation.

To measure the anatomical traits in seven selected samples, the method described by von Arx et al., (2016) was used. Each increment core was cut into 4-5 cm long pieces and put in distilled water for 10 minutes to soften the cells and avoid damage to the cell structure during cutting. However, care was taken to avoid the samples being too soft; the use of tissue paper to absorb excess moisture prevented micro-section fissures during cutting. 12 µm thick transverse micro-

sections were cut perpendicularly to axially oriented xylem cells with a rotary microtome (Leica RM2245, Heidelberg, Germany) using Feather N35 blades (Feather Safety Razor Co., Ltd, Osaka, Japan). To avoid disrupting the delicate anatomical structures, the microtome blade was frequently replaced. For each sample, three glass slides were prepared with each glass slide containing two micro-sections. Having six micro-sections per sample offered the opportunity of choosing the best micro-section for image processing and to have backup samples in any unforeseen event of sample loss.

To make a permanent slide, and to increase contrast, the micro-sections were stained with safranin (1% in distilled water) - for lignified tissues, and astrablue (0.5% in dist. water) - for non-lignified tissues. After about 10 mins, the sections were de-stained, first with distilled water and thereafter, dehydrated sequentially using 50% ethanol and absolute ethanol (100%). When completely de-stained (presence of clear solvent), the sections were dried using tissue towel and permanently fixed on glass slides using Eukitt (BiOptica, Milan Italy). The permanent fixing was done immediately after drying to prevent micro-sections from flaking and folding. The resulting microslides were put in between two strips of heat-resistant plastics, placed on a metal plate, and a magnetic bar (acting as weight) was placed on top to keep the sections flat during the drying phase. The slides were allowed to air-dry at room temperature for some days (between 10 to 14 days). When drying was difficult, sections were put in the oven at 60^{o}C for 12 hours. To get a clear image devoid of pollution and distortion, the microslides were thoroughly cleaned of dried Eukitt by scrapping with old blades and wiping with a clean lens towel.

2.3 Anatomical traits measurement

Digital images were captured using digital automated microscope Axio Scan.Z1 (Zeiss, Jena, Germany) at 100× magnification with a resolution of 2.27 pixels/µm. ROXAS v3.0.634 (von Arx & Carrer, 2014), an image analyses software that measures different xylem traits, was used for the image analysis. Images (Figure 2) were grouped into automatic areas of interest (auto-AOI) and manual AOI (manual-AOI) configurations depending on the possibility to perform automatic detection of the Area of Interest in the software. A batch run was performed on the auto-AOI and manual-AOI samples to automatically detect and measure all cells in the image.

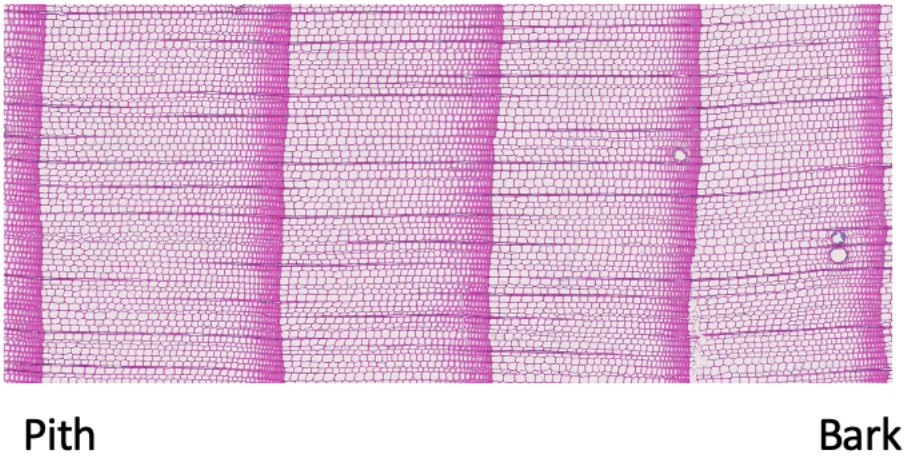

Figure 2: An image of 12 µm thick wood section after coloration in safranin and astra-blue.

After running the samples in batch mode, each was manually edited on ROXAS. The process was done to optimize the quality of results and to eliminate deficiencies in the images (von Arx et al., 2016). Specifically, the following defects were corrected: broken cells, split cells, joined cells, multiple borders, outlier borders and cells, selected parenchyma rays, xylem pits, and resin ducts.

To accurately date the sample tree rings, the mean ring width (MRW) obtained from ROXAS software was cross-matched with the ring width recorded by TsapWin, previously checked in COFECHA. The year of each ring in the sample was dated (Figure 3) when a match exists in values and trends between ROXAS output (MRW) and Tsap ring width values (Figure 4).

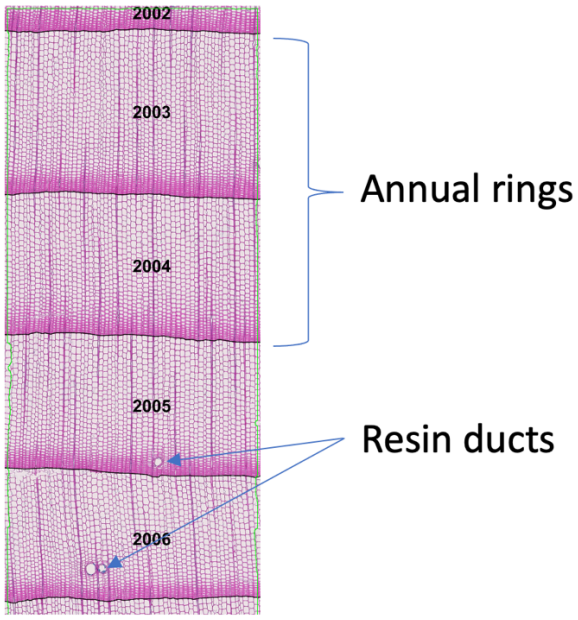

Figure 3: An image of a dated tree rings. Objects like resin ducts were manually removed from the image in ROXAS.

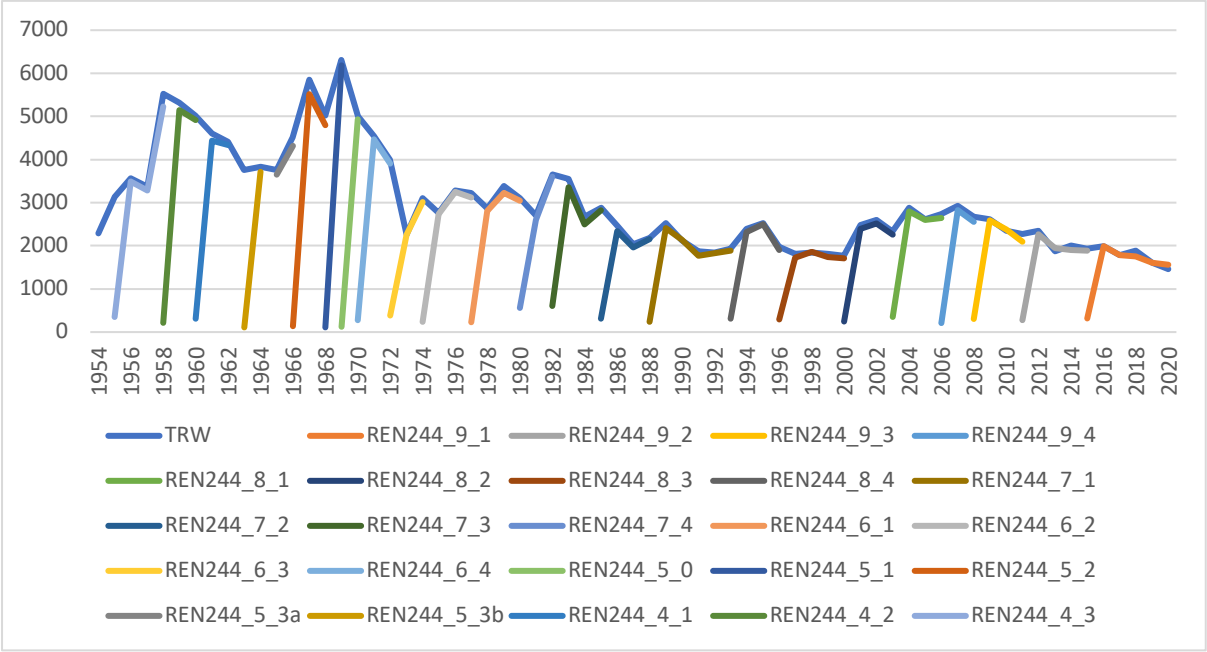

Figure 4: Cross-matched tree ring widths used for accurate dating of samples.

The last procedure in ROXAS was the computation of the cell wall thickness (CWT) in batch mode.

2.4 Chronology building

Cell number (NUM) and cell wall area (CWA) (Figure 5) were calculated by ROXAS. For cases where CWA was negative in the ROXAS output, i.e., the cell wall thickness for 4 sides of the cell was incomplete, CWA was recalculated in R from the available information on cell lumen diameter and cell wall thickness.

The corrected cell wall area (CWA) and the cell number (NUM) for earlywood (EW) and latewood (LW) of each year were determined. The Mork's index (= 2 × double cell wall thickness/cell lumen) was used to group the cells into EW (Mork's index values below 1) and LW (Mork's index values above 1) (Figure 6).

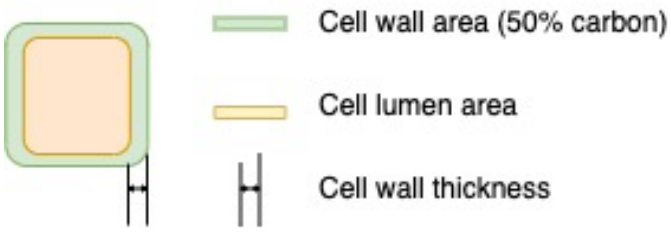

Figure 5: An illustration showing the cell wall area (CWA) of a xylem cell.

Since C concentration in the wood of temperate conifers is quite constant and very close to 50% (50.1% ± 0.4, Martin et al., 2018), the CWA, as the biomass estimate based on the xylem structure, is a very reliable estimate of the C amount in the cell.

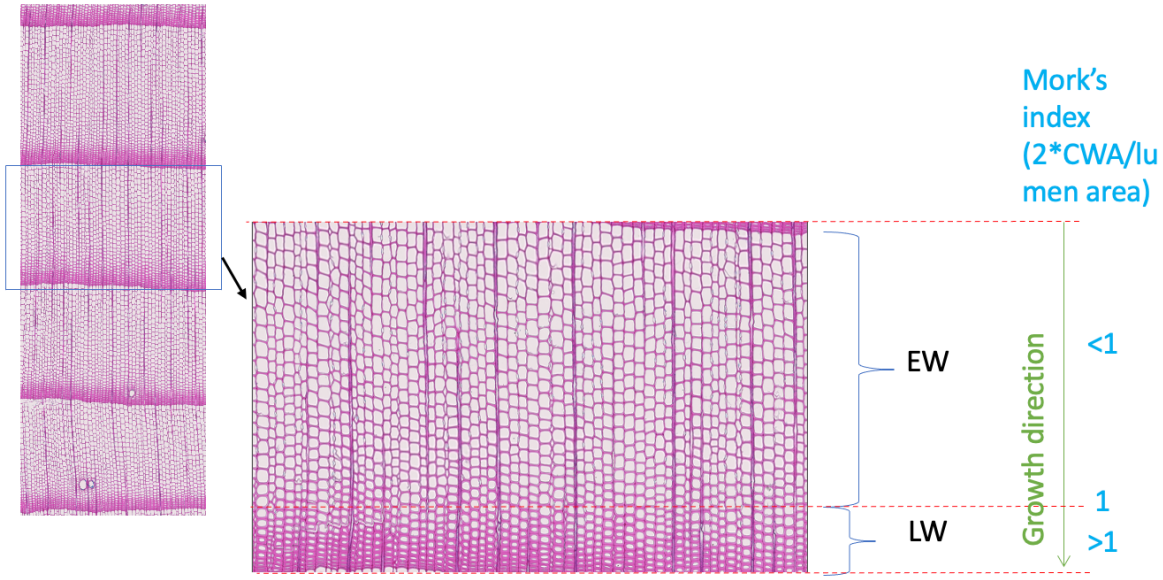

Figure 6: A depiction of the earlywood and latewood based on the Mork's index

The size and age trends in all the anatomical series were detrended using a 15-year cubic smoothing spline (Carrer et al., 2015; Cook and Kairiūkštis, 1990). The mean standardized chronologies for CWA and for NUM in the EW and LW were built using the R package dplR (Bunn, 2008).

2.5 Eddy covariance dataset processing

The eddy covariance primary datasets were collected and processed by Professor Leonardo Montagnani of the University of Bozen. The datasets were collected using the method described by (Liu et al., 2021). A continuous half-hourly measurement of EC variables (Table 2) was integrated over 60 minutes.

Table 2: The eddy covariance variables.

Eddy covariance variable	Description
CO2 (µmolCO2 mol−1)	Carbon Dioxide (CO2) mole fraction in moist air
FC (µmolCO2 m−2 s−1)	Carbon Dioxide (CO2) turbulent flux (without storage component)
SC (µmolCO2 m−2 s−1)	Carbon Dioxide (CO2) storage flux measured with a vertical profile system
USTAR (m s−1)	Friction velocity
H (W m−2):	Sensible heat turbulent flux, without storage correction
LE (W m−2)	Latent heat turbulent flux, without storage correction
WS (m s−1)	Horizontal wind speed
TA (deg C)	Air temperature
NETRAD (W m−2)	Net radiation - needed for energy balance closure
RH (%)	Relative humidity (range 0–100%)
PA (kPa)	Atmospheric pressure
G (W m−2)	Ground heat flux, not mandatory, but needed for the energy balance closure calculations
TS (deg C)	Soil temperature
SW_IN (W m−2)	Incoming shortwave radiation
SW_IN_POT (W m−2)	Potential incoming shortwave radiation (top of atmosphere theoretical maximum radiation)
PPFD_IN (µmolPhotons m−2 s−1)	Incoming photosynthetic photon flux density
P (mm)	Precipitation total of each 30 or 60-minute period
LW_IN (W m−2)	Incoming (down-welling) longwave radiation
SWC (%)	Soil water content (volumetric), range 0–100%

Source: (Pastorello, 2020)

These datasets were subjected to quality control protocols and data processing pipeline as described by (Pastorello, 2020). The NEE = -NEP, was filtered with an ensemble of USTAR thresholds: constant USTAR threshold (CUT) and variable USTAR threshold (VUT), using the nighttime and daytime methods (Lasslop et al., 2010; Reichstein et al., 2005). Also, the protocol enabled the gap-filling of meteorological and flux measurements using the marginal distribution sampling (MDS) method (Reichstein et al., 2005) and finally, the NEE was

partitioned into ecosystem respiration (Reco) and photosynthesis (gross primary production) in line with the two methods (Liu et al., 2021). The processed GPP of the daytime and nighttime methods downloaded from the ICOS open access database were used in this study.

2.6 Statistical analyses

The GPP from the two methods (daytime and nighttime) were correlated with the mean temperature and precipitation at Renon from 1999 to 2020 using the temperature and precipitation data obtained from the E-OBS climate database (lon = 11.25 to 11.50, lat = 46.50 to 46.75) (Cornes et al., 2018).

The temperature data were categorized into annual, summer, autumn, and spring while the precipitation data were regrouped into autumn, winter, spring and summer. The winter precipitation was calculated by taking the average monthly value in December of the previous year with the January and February of the current year.

In the same vein, the correlation between xylem anatomical traits (CWA and NUM for EW and LW) was calculated. All the years covered in the sample anatomical series (1934-2020) were correlated with temperature and precipitation data (1934-2020).

Lastly, the xylem chronology (CWA and NUM for EW and LW) were correlated with the EC GPP (Nighttime and daytime separately). In this instance, the GPPs were classified into the annual, winter, spring, summer and autumn GPP. Due to shorter time series of EC data compared to climate data, the xylem chronology from 1999 to 2020 was correlated with EC GPP from 1999 to 2020.

3. RESULTS

3.1 Site Climate

The climatic data of the site obtained from the E-OBS climate database (lon = 11.25 to 11.50, lat = 46.50 to 46.75) (Cornes et al., 2018), showed that the annual mean temperature of the site is on a steady increase in the last 100 years (Figure 7). The retrieved and processed data covered from 1920 to 2020.

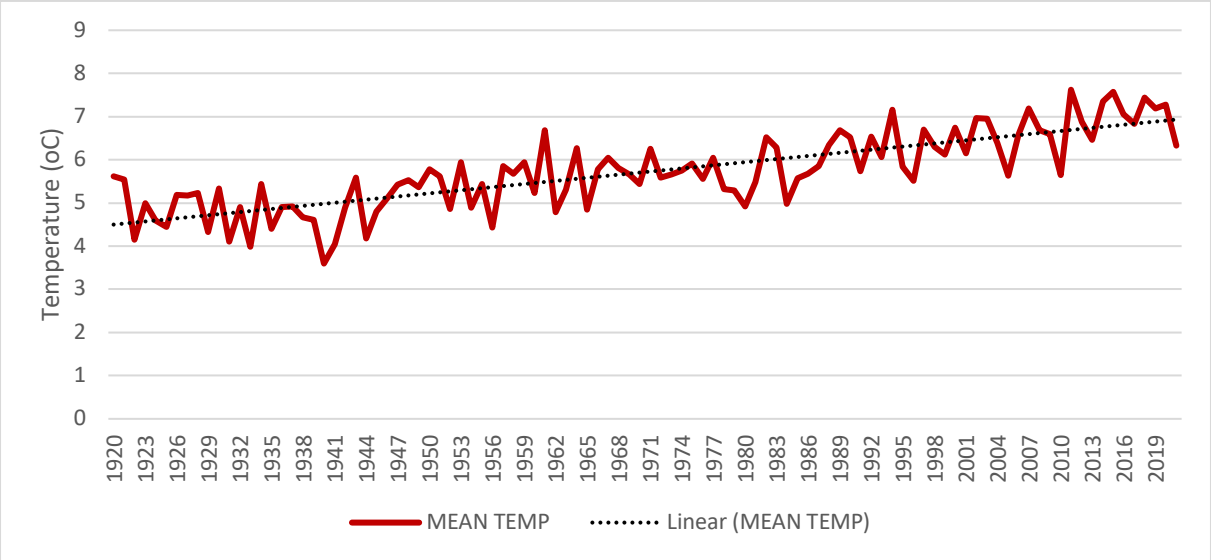

Figure 7: The annual mean temperature of Renon site.

Source: the E-OBS climate database (Cornes et al., 2018).

Conversely, the annual mean precipitation showed a steady trend (Figure 8).

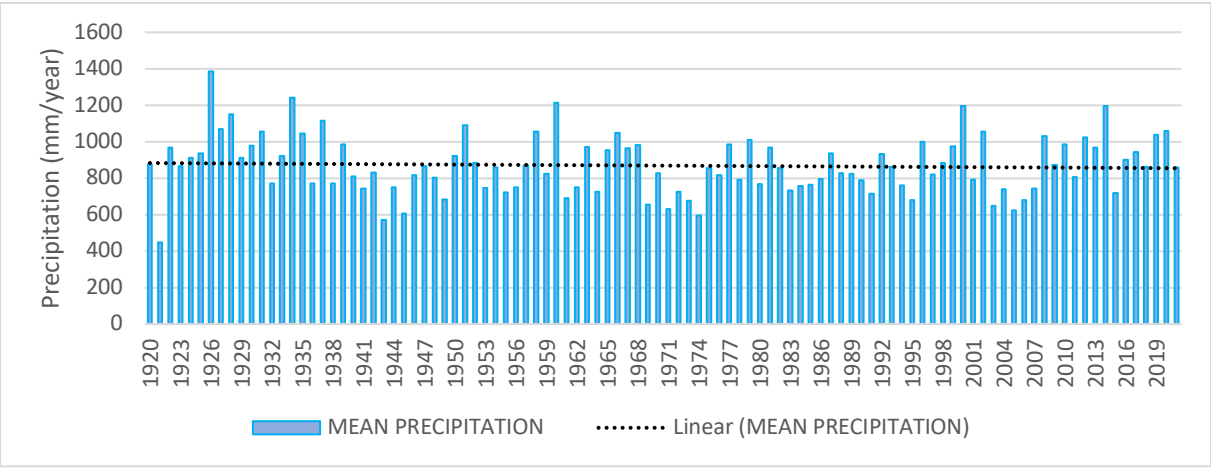

Figure 8: The annual mean precipitation of Renon site.

Source: the E-OBS climate database (Cornes et al., 2018)

3.2 Xylem anatomy chronologies

The boxplot of CWA (Figure 9) showed that there was no difference between EW and LW. On the opposite, NUM (Figure 10) was different between EW and LW.

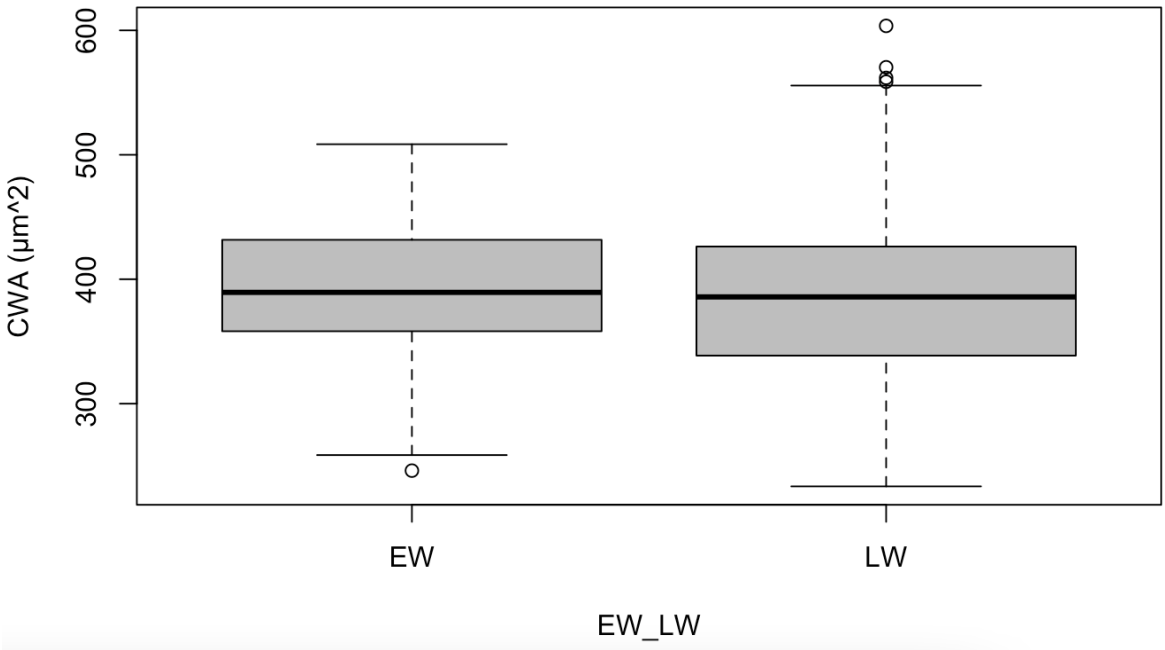

Figure 9: CWA in earlywood (EW) and latewood (LW).

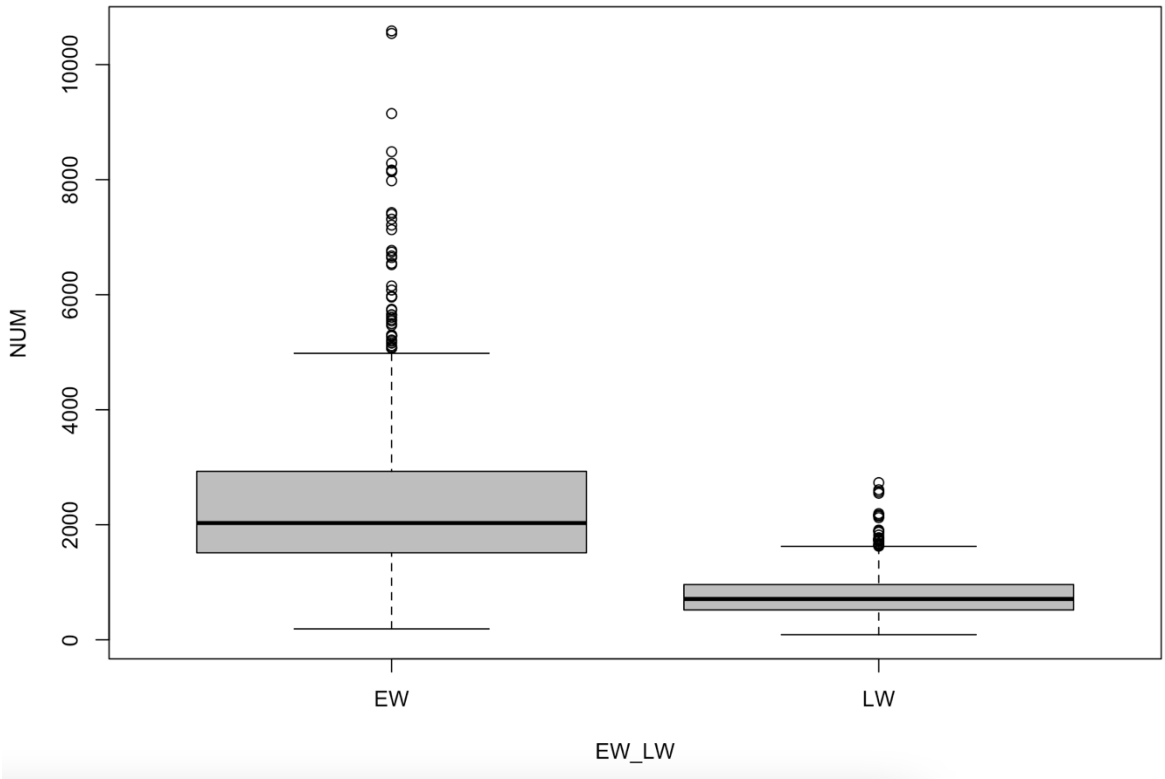

Figure 10: NUM in earlywood (EW) and latewood (LW).

The anatomical detrended chronologies from 1934 to 2020 showed that CWA and NUM varied more in LW than EW (Figure 11).

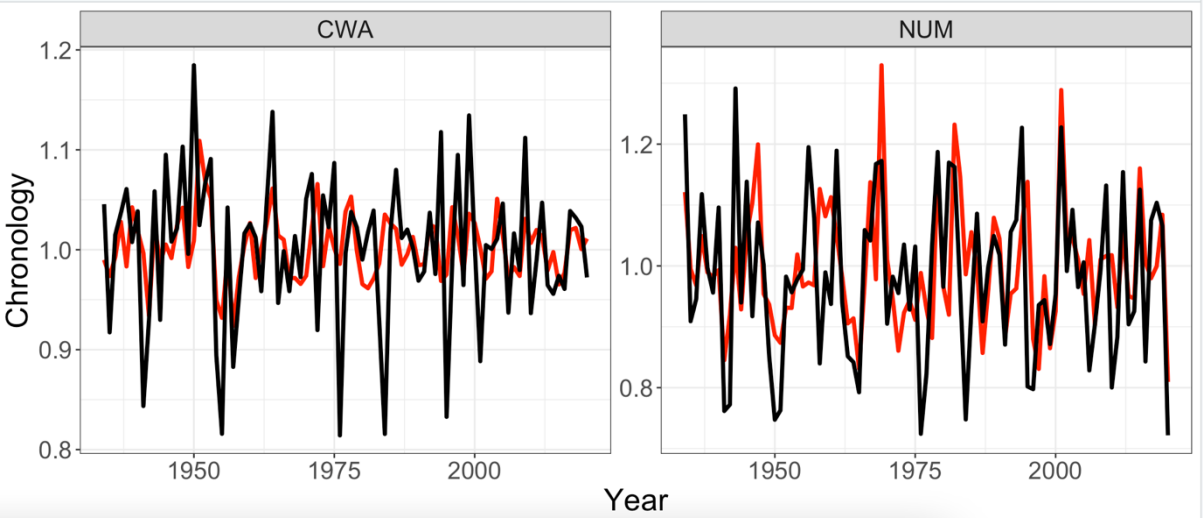

Figure 11: The standardized anatomical series.

The red colour shows the annual variability in earlywood (EW) while the black shows that of latewood (LW).

This was confirmed with an F-test on the chronology variability (Table 3).

Table 3: Fischer test for variance between xylem anatomy traits.

F-Test Two-Sample for Variances

	CWA_EW	*CWA_LW*	*NUM_EW*	*NUM_LW*
Mean	1.00235149	1.00161765	0.99502954	0.98167167
ST. DEV.	0.03222973	0.07198201	0.09987547	0.13416833
Variance	0.00103876	0.00518141	0.00997511	0.01800114
Observations	87	87	87	87
df	86	86	86	86
F	0.20047732		0.55413761	
P(F<=f) one-tail	7.1765E-13		0.00336438	
P Two-tail	1.4352E-12		0.00672876	
F Critical one-tail	0.69997751		0.69997751	

Pearson correlation showed a positive association between the CWA_EW and CWA_LW; NUM_LW and CWA_LW, and NUM_EW and NUM_LW (P<0.01). Conversely, a negative correlation existed between CWA_EW and NUM_EW (Table 4).

Table 4: Pearson correlation between the cell wall area (CWA) and cell number (NUM) chronologies.

Colours indicate the direction and strength of association, from dark red (strong negative) to dark blue (strong positive) correlations. Bold indicates significant correlations.

	CWA_EW	*CWA_LW*	*NUM_EW*	*NUM_LW*
CWA_EW	1.000			
CWA_LW	**0.402**	1.000		
NUM_EW	**-0.300**	-0.135	1.000	
NUM_LW	-0.148	**0.314**	**0.509**	1.000

3.3 Eddy covariance data

The GPP of Renon forest (Figure 12) showed different annual values based on the methods and the USTAR threshold used.

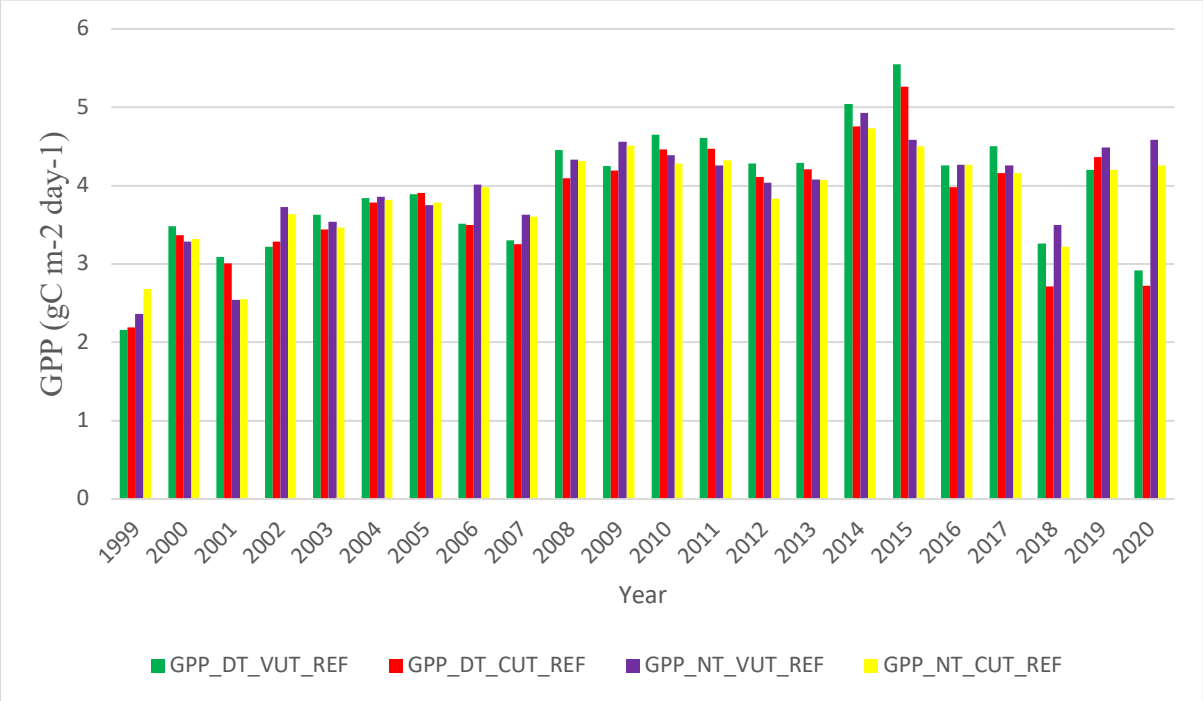

Figure 12: The mean daily GPP of Renon forest obtained using two methods, the daytime (DT) and nighttime (NT) and two USTAR thresholds, variable USTAR threshold (VUT) and constant USTAR threshold (CUT).

The different methods, on average, showed similar increasing patterns in the study period but few showed a decrease in the last three years such as the GPP_DT_CUT_REF and GPP_DT_VUT_REF. Besides the common interannual variability, each year showed a dissimilar rank for example GPP_DT_VUT_REF and GPP_DT_CUT_REF peaked in 2015, towering above GPP_NT_CUT_REF and GPP_NT_VUT_REF but both decreased in 2020, much lower than GPP_NT_CUT_REF and GPP_NT_VUT_REF. Apparently, different methods can provide quite different results.

3.4 Correlation between GPP and climate

The monthly averages of GPP and temperature (Figure 13) showed that along the year course, GPP increases with temperature with the highest values in summer, from May to September, and maximum value in July.

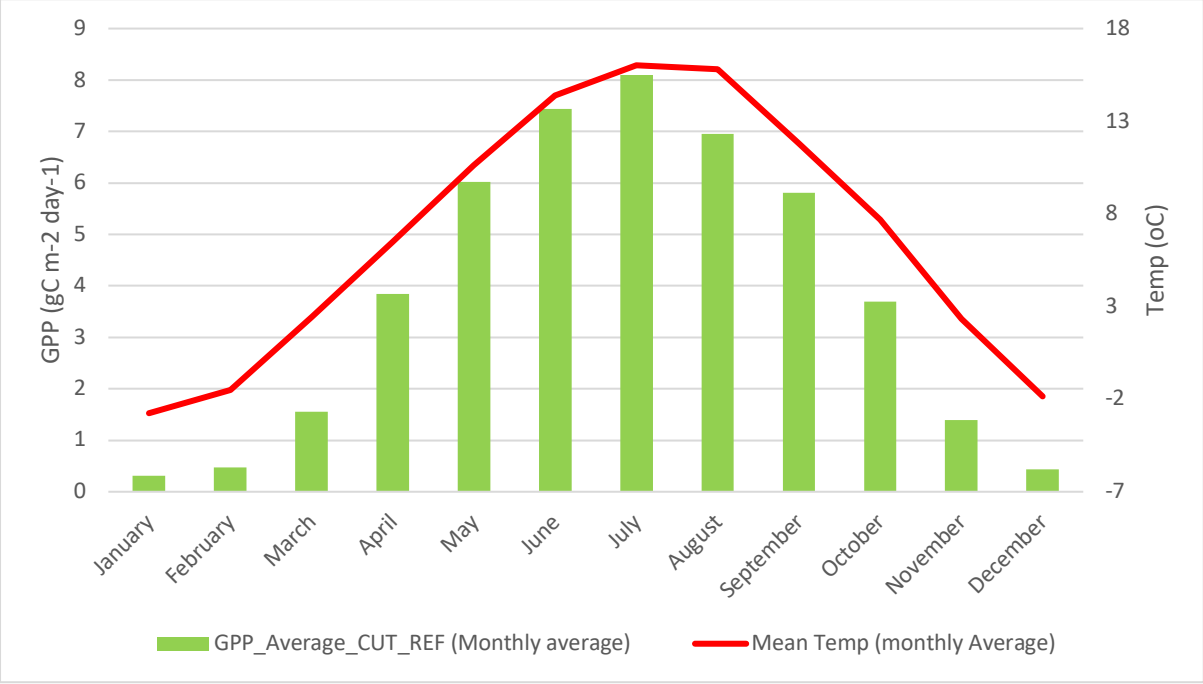

Figure 13: The monthly average of GPP and the temperature of Renon site.

In the same vein, GPP annual variation followed the precipitation pattern. The highest precipitation was recorded in August (Figure 14).

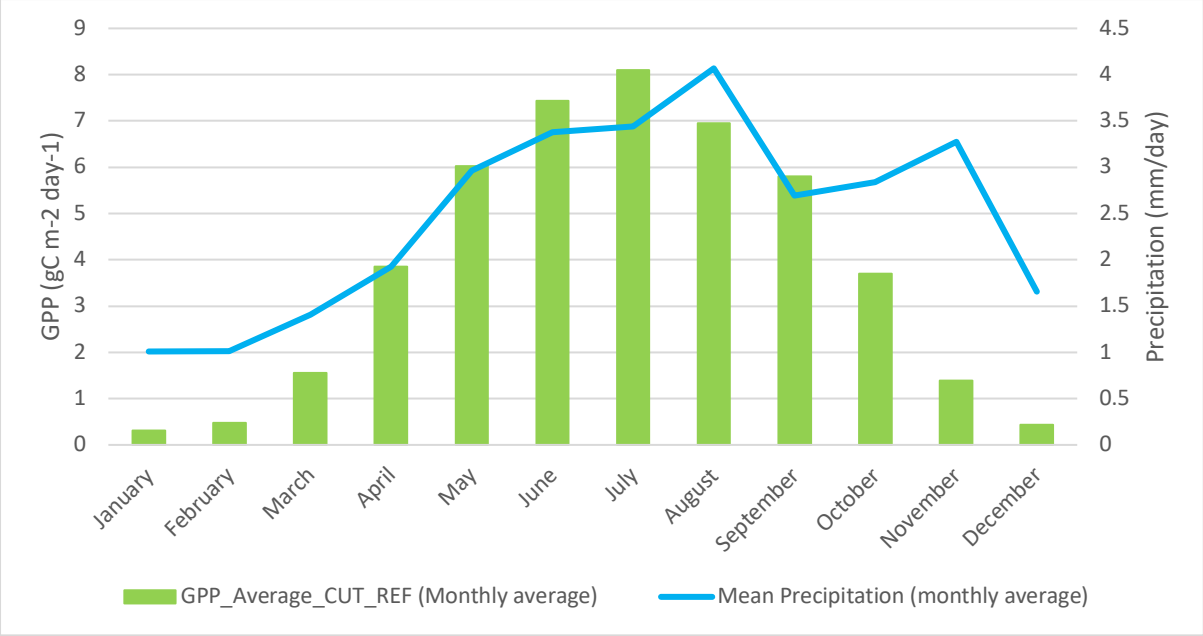

Figure 14: The monthly averages of GPP and precipitation at Renon forest.

The Pearson correlation between temperature and precipitation of the current year and GPP inter-annual variability showed variable results with some significant but probably spurious correlations, especially with precipitation (Table 5). Indeed, in some cases monthly GPP was associated to climate in successive months.

Table 5: Correlation between the mean monthly GPP with temperature and precipitation from January to December.

Colours indicate the direction and strength of association, from dark red (strong negative) to dark blue (strong positive) correlations. Bold indicates significant correlations.

		GPP											
		JAN	FEB	MAR	APR	MAY	JUN	JUL	AUG	SEP	OCT	NOV	DEC
Temperature	Jan	0.109	0.096	0.122	0.148	-0.301	-0.364	-0.195	-0.398	-0.341	-0.084	-0.201	-0.087
	Feb	0.051	0.039	0.269	0.320	0.054	-0.131	-0.024	-0.112	-0.002	-0.021	0.188	0.225
	Mar	-0.019	-0.011	**0.564**	0.243	-0.067	-0.157	0.100	-0.146	-0.028	0.209	0.275	0.008
	Apr	0.023	-0.128	-0.125	**0.486**	0.278	0.024	-0.056	-0.185	-0.172	-0.089	-0.201	-0.053
	May	0.054	0.014	0.005	-0.154	-0.193	-0.371	-0.116	-0.574	-0.371	-0.267	-0.231	-0.444
	Jun	0.004	0.058	0.301	0.107	0.015	0.168	0.189	0.198	0.102	0.153	0.133	0.228
	Jul	0.259	0.228	0.094	0.241	0.094	0.409	0.225	0.149	0.046	-0.075	-0.259	-0.032
	Aug	0.115	0.119	0.097	0.037	0.021	0.034	0.158	-0.180	-0.160	0.106	-0.046	-0.137
	Sep	-0.069	-0.143	-0.245	0.108	0.264	0.094	-0.121	-0.052	-0.182	-0.182	-0.022	0.121
	Oct	-0.033	-0.067	-0.083	-0.302	-0.416	-0.280	0.153	0.169	0.309	**0.464**	0.156	0.262
	Nov	0.297	0.269	0.461	0.366	0.243	0.366	0.237	-0.045	0.087	0.113	0.209	0.016
	Dec	0.611	0.539	0.507	0.322	-0.049	0.223	-0.073	-0.090	-0.023	-0.069	0.263	**0.632**
Precipitation	Jan	-0.053	-0.057	-0.060	-0.008	-0.241	-0.053	0.296	0.088	0.302	0.462	0.159	-0.033
	Feb	-0.143	-0.192	-0.039	0.210	0.200	0.266	0.218	0.304	0.470	0.294	0.385	0.144
	Mar	0.061	-0.033	-0.182	-0.334	-0.437	-0.366	-0.214	-0.344	-0.107	-0.021	-0.159	0.126
	Apr	-0.184	-0.098	-0.008	-0.325	-0.231	-0.127	0.050	0.086	0.183	0.280	0.250	0.237
	May	0.220	0.310	0.324	-0.038	-0.192	0.118	0.002	0.129	-0.020	0.009	0.006	0.382
	Jun	-0.052	-0.086	0.189	0.284	0.131	-0.205	0.083	-0.347	-0.235	-0.082	0.192	-0.165
	Jul	-0.037	0.028	0.174	-0.001	0.033	-0.037	0.115	-0.009	0.227	0.205	0.608	0.069
	Aug	-0.073	-0.151	-0.148	0.202	0.211	-0.024	-0.222	-0.398	-0.370	-0.428	-0.434	-0.280
	Sep	0.143	0.227	0.280	0.146	0.114	-0.034	0.223	-0.115	-0.024	0.117	0.169	-0.008
	Oct	0.240	0.207	-0.114	-0.307	-0.171	-0.153	-0.310	-0.355	-0.352	-0.162	-0.228	0.151
	Nov	-0.050	0.041	0.327	-0.124	-0.112	0.128	-0.113	0.103	0.149	0.159	0.269	0.437
	Dec	-0.236	-0.229	-0.316	0.007	0.487	0.248	0.029	-0.056	0.052	-0.229	-0.183	-0.368

Nevertheless, significant and positive correlations were obtained between March and April temperatures with March and April GPP respectively (Figure 15).

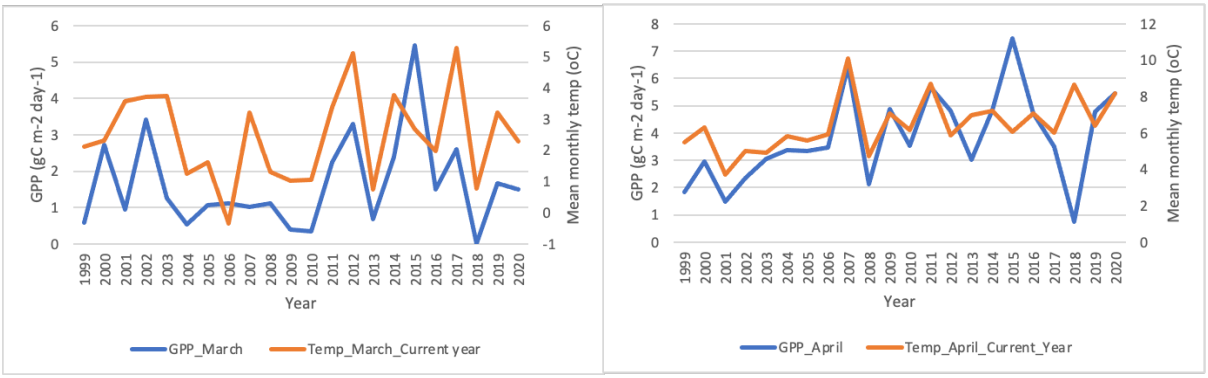

Figure 15: Variation of March (left panel) and April (right panel) GPP and March and April temperature of the current year along the study period.

Interestingly, no correlation was observed when the temperature of the previous year was correlated with the GPP of the current year (Annex 1).

3.5 Correlation between xylem anatomical series and climate

The Pearson correlation ($P<0.05$) between anatomical series and monthly mean temperature showed that the NUM_LW had a significant positive relationship with March and August temperatures. Likewise, CWA_LW correlated significantly with May, August, and September temperatures (Table 6). It was observed too that the NUM_EW correlated positively with October temperature.

Table 6: Pearson correlation between anatomical chronologies and temperature.

Colours indicate the direction and strength of association, from dark red (strong negative) to dark blue (strong positive) correlations. Bold indicates significant correlations.

Temperature	CWA_EW	CWA_LW	NUM_EW	NUM_LW
Jan	-0.108	-0.051	-0.051	0.012
Feb	-0.114	-0.117	0.043	-0.095
Mar	-0.113	0.122	0.104	**0.356**
Apr	0.088	0.100	-0.149	0.025
May	0.095	**0.314**	0.176	0.188
Jun	-0.023	0.131	-0.003	0.012
Jul	-0.075	0.045	**0.249**	-0.095
Aug	0.096	**0.294**	0.002	**0.222**
Sep	-0.111	**0.359**	-0.042	0.096
Oct	-0.133	-0.174	**0.319**	0.144
Nov	-0.062	-0.004	0.067	0.009
Dec	-0.021	-0.074	-0.057	-0.031
Aug+Sep	-0.016	**0.435**	-0.028	0.207
May-Sep	-0.006	**0.391**	0.125	0.146

By merging months when xylem formation is expected (from May to September, Rossi et al., 2003), we increased positive correlation between CWA_LW and the average of August and September temperatures and the average of May to September temperatures (Table 6). When comparing the two time series, a few common peaks and trend were evident (Figure 16).

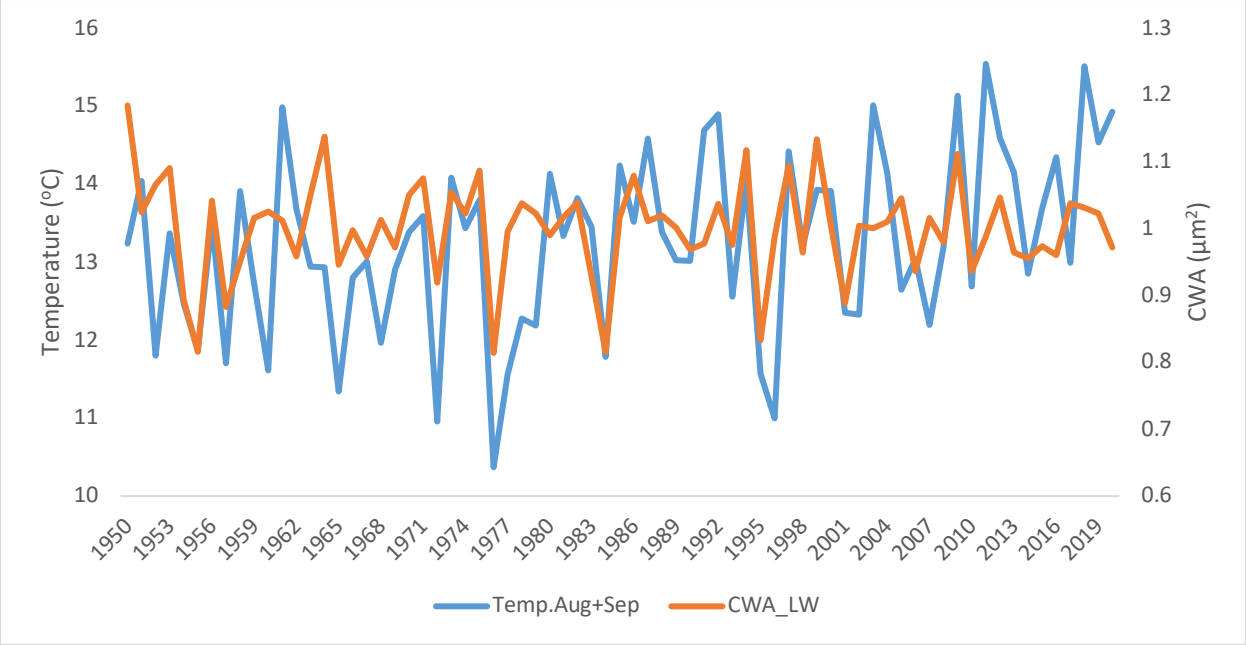

Figure 16: Variation of CWA and May to September temperature from 1950 to 2020.

With precipitation, the CWA_EW showed a positive relationship (P<0.05) with March precipitation whereas the CWA_LW showed a positive correlation with the April precipitation (Table 7).

Table 7: Pearson correlation between the anatomical chronologies and precipitation.

Colours indicate the direction and strength of association, from dark red (strong negative) to dark blue (strong positive) correlations. Bold indicates significant correlations.

Precipitation	CWA_EW	CWA_LW	NUM_EW	NUM_LW
Jan	0.163	0.050	0.088	0.067
Feb	0.190	-0.076	-0.062	-0.167
Mar	**0.228**	0.072	0.041	0.038
Apr	0.069	**0.254**	0.022	0.090
May	-0.222	**-0.308**	0.078	-0.100
Jun	-0.036	0.103	-0.167	0.046
Jul	-0.078	-0.002	-0.147	0.173
Aug	0.064	0.132	-0.115	**-0.225**
Sep	-0.037	-0.170	0.020	-0.064
Oct	0.126	0.010	-0.112	-0.054
Nov	0.056	0.100	-0.029	-0.050
Dec	0.001	0.062	0.001	-0.159

Also, negative correlations were observed between the CWA_LW and May precipitation, and between NUM_LW and August precipitation (Table 7).

3.6 Correlation between the anatomical series and the GPP

A significant correlation (P<0.05) existed between the CWA_LW and the October GPP of the daytime method using constant USTAR threshold while a marginal positive correlation was obtained between NUM_EW and June to September GPP (
Table 8).

Table 8: Pearson correlation between anatomical chronologies and GPP obtained with the constant USTAR threshold (CUT).

(A) showed the GPP using the daytime and (B) is the GPP using the night-time method. Colours indicate the direction and strength of association, from dark red (strong negative) to dark blue (strong positive) correlations. Bold indicates significant correlations.

GPP_DT_CUT	*CWA_EW*	*CWA_LW*	*NUM_EW*	*NUM_LW*
Jan	-0.228	-0.141	0.182	0.121
Feb	-0.280	-0.172	0.251	0.145
Mar	-0.336	-0.095	0.221	0.233
Apr	-0.196	-0.032	-0.118	-0.164
May	0.002	-0.088	-0.285	-0.354
Jun	-0.232	-0.185	0.126	-0.063
Jul	-0.133	-0.145	0.353	0.299
Aug	-0.105	-0.121	0.296	0.109
Sep	-0.168	-0.250	0.306	0.211
Oct	0.022	-0.134	0.414	**0.465**
Nov	-0.095	-0.231	0.155	0.065
Dec	-0.147	-0.077	0.096	-0.024

(A)

GPP_NT_CUT	*CWA_EW*	*CWA_LW*	*NUM_EW*	*NUM_LW*
Jan	0.206	0.181	**-0.434**	-0.377
Feb	-0.139	-0.229	-0.116	-0.201
Mar	-0.340	-0.210	0.204	0.136
Apr	-0.239	-0.111	-0.215	-0.320
May	-0.149	-0.109	-0.261	-0.377
Jun	-0.212	-0.044	-0.140	-0.172
Jul	-0.042	0.248	-0.210	-0.116
Aug	-0.088	-0.021	-0.061	-0.171
Sep	-0.006	-0.175	-0.013	-0.140
Oct	-0.118	-0.231	0.303	0.281
Nov	-0.049	-0.310	-0.204	-0.315
Dec	-0.301	-0.201	-0.076	-0.101

(B)

Similarly, the GPP obtained using variable USTAR threshold (VUT) showed positive correlations between the anatomical series (emphasis on NUM_EW and NUM_LW) and June to October GPP but non-significantly (Table 9).

Table 9: Pearson correlation between anatomical chronologies and the GPP obtained with the variable USTAR threshold (VUT).

(A) showed the GPP using the daytime and (B) is the GPP using the night-time method. Colours indicate the direction and strength of association, from dark red (strong negative) to dark blue (strong positive) correlations. Bold indicates significant correlations.

GPP_DT_VUT	*CWA_EW*	*CWA_LW*	*NUM_EW*	*NUM_LW*
Jan	-0.322	-0.169	0.164	0.139
Feb	-0.256	-0.101	0.240	0.220
Mar	-0.304	-0.142	0.198	0.209
Apr	-0.221	-0.101	-0.169	-0.201
May	-0.064	-0.158	-0.207	-0.297
Jun	-0.293	-0.252	0.187	-0.014
Jul	-0.190	-0.233	0.372	0.269
Aug	-0.215	-0.178	0.315	0.129
Sep	-0.158	-0.177	0.310	0.267
Oct	0.112	-0.108	0.379	0.415
Nov	0.117	-0.076	0.048	0.213
Dec	0.086	-0.117	-0.187	-0.245

(A)

GPP_NT_VUT	*CWA_EW*	*CWA_LW*	*NUM_EW*	*NUM_LW*
Jan	0.183	-0.142	-0.290	-0.355
Feb	-0.069	-0.255	-0.183	-0.254
Mar	-0.323	-0.236	0.182	0.102
Apr	-0.264	-0.136	-0.206	-0.319
May	-0.217	-0.145	-0.243	-0.343
Jun	-0.212	-0.013	-0.116	-0.118
Jul	-0.101	0.184	-0.189	-0.105
Aug	-0.105	-0.054	-0.071	-0.112
Sep	-0.038	-0.251	-0.006	-0.092
Oct	-0.085	-0.195	0.331	0.329
Nov	-0.020	-0.302	-0.099	-0.294
Dec	-0.249	-0.187	-0.066	-0.189

(B)

Comparatively, the daytime-CUT method showed a higher correlation than daytime VUT method and on a general basis, the daytime methods had a better correlation between the anatomical series and GPP than the night-time methods.

At the seasonal level, a marginal correlation was obtained when the GPP_DT_CUT was correlated with anatomical series (

Table 10). Marginal positive associations were observed for summer and autumn.

Table 10: The correlation between anatomical series and seasonal GPP

GPP_DT_CUT	CWA_EW	CWA_LW	NUM_EW	NUM_LW
Winter	-0.259	-0.156	0.215	0.109
Spring	-0.230	-0.087	-0.081	-0.126
Summer	-0.182	-0.177	0.313	0.149
Autumn	-0.100	-0.231	0.356	0.307

4. DISCUSSION

This thesis used dendroanatomy, i.e. the analysis of wood anatomical traits along series of dated tree rings (Pacheco Solana et al., 2018), to understand the complementarity between the forest carbon uptake (as measured with eddy covariance) and the tree biomass growth at the Renon forest in the Italian Alps.

4.1 Climate and wood anatomy

Analysis of the site climate pointed out clearly that the annual mean temperature is increasing at the study site which is in consonance with the observed warming in the Alps (Gobiet et al., 2014). This evident warming lends credence to the prevailing environmental issue of climate change and calls for studies on the complex relationships between climate, forest productivity, and tree growth. On the contrary, the annual mean precipitation has remained relatively constant. The 100-year climate data has shown that the annual variability was higher with temperature than precipitation and is in line with the temperature and precipitation in the Italian Alps (Montagnani et al., 2009).

Results of the quantitative wood anatomy analysis showed no difference between the mean values of CWA_EW and CWA_LW, indicating that the biomass (and therefore of carbon amount) of cells in earlywood and latewood was similar. As expected, the number of cells was much larger in earlywood (wider) than in latewood. After standardization, the cell wall area (CWA) and the number of cell (NUM) were more variable in latewood than in earlywood. This could be associated with varying environmental factors within the growing season and the different duration of formation of tracheid cells in the early and late season (Rossi et al., 2006). Looking at the Pearson correlation among these parameters, a positive relationship was observed between the CWA_EW and CWA_LW, NUM_EW and NUM_LW, and CWA_LW and NUM_LW. Conversely, a negative association was observed between CWA_EW and NUM_EW. By implication, any favourable growth year would be reflected in the EW and LW but a mutual incompatibility exists between CWA_EW and NUM_EW. Perhaps these findings are due to the different physiological and sequential mechanisms underpinning xylem formation. NUM is linked to the number of cambial cells and the formation starts from mid-May to Mid-August whereas the CWA is interconnected to the successive phases of cell wall enlargement and cell wall thickening, which start around May to June and end in September (Rossi et al., 2006). Furthermore, as indicators of forest productivity, these anatomical traits

are subjective to meteorological conditions (Anić et al., 2018; Fritts, 1976). To that effect, we went further to examine the connection between these anatomical traits and the climate.

A significant association exists between the CWA_LW and late summer temperatures (August and September). In the same vein, a positive relationship was observed with the temperatures of the entire growing season (May to September). This result is in line with previous findings on the same species at similar elevation (Castagneri et al., 2017), xylogenetic studies in the Alps (Rossi et al., 2006), and worldwide observations on tree ring maximum density, which is determined by the latewood cell wall thickness (Björklund et al., 2017). As CWA is linked to cell wall formation, it is essentially the accumulation of carbon, and this process occurs at the end of the growing season in latewood. The observed positive link between CWA_LW with late summer and growing season temperature indicates that carbon accumulation in woody biomass at the end of the growing season (wall thickening in latewood) depends on the growing season temperature (Lempereur et al., 2015; Rossi et al., 2006).

On a seasonal level, there was generally a positive correlation between annual mean, spring, summer, and autumn temperatures with CWA_LW, NUM_EW, and NUM_LW, pointing to the fact that a typical warm year would benefit xylem formation and thus carbon accumulation in woody biomass at the site (Crabbe et al., 2016).

On the other hand, the CWA_EW showed a positive relationship with precipitation in the months of October (previous year) to April (current year). Obviously, these are winter periods with precipitation in form of snow. The plausible reason for this correlation is that snow makes water available along the successive growing season (Zeeman et al., 2017).

From the foregoing, CWA_EW responds quite positively to precipitation while NUM_EW, CWA_LW, and NUM_LW are strongly influenced by temperature (Annex 2). These agree with the observed biophysical control factors of cambial activity and align with the proposition that sink-limitation is stronger than source-limitation in carbon assimilation and tree growth (Cabon et al., 2022).

4.2 Climate influence on GPP

The two methods and the two USTAR thresholds showed important differences in the quantification of annual GPP. The annual variability in GPP is expected due to varying environmental conditions (Anić et al., 2018; Niu et al., 2011) but the discrepancy in the two methods highlights the complexity of EC flux measurement (Babst et al., 2014b). The difference could be related to the protocols involved. The Night-time method uses night-time data to parameterize a respiration-temperature model which is then used to obtain the

ecosystem respiration (Reco). After which, the GPP would be determined as the difference between net ecosystem exchange (NEE) and Reco. On the other hand, the daytime method uses daytime and night-time data to obtain the model parameters. One part of which depends on a light-response curve and vapour pressure deficit for GPP while the second part is based on the respiration-temperature relationship. Therefore, the daytime method enables NEE to become a function of both GPP and Reco, both obtained from the model (Pastorello, 2020).

The seasonal course of GPP showed a direct relationship with climatic factors. GPP increases from March and drops around October so also the temperature. These months are the most favourable time for tree species growing in temperate regions at this elevation, due to the availability of high temperature required for photosynthesis Seyednasrollah et al., 2021; Wehr et al., 2016).

The analyses showed a positive link between the temperature of March, April, October and December with the GPP of March, April, October and December. In particular the close association between temperature and GPP in March and April showed that the variability of spring temperature, which is generally above 0 ^{o}C at this elevation, is sufficient to initiate photosynthesis and in general critical for the carbon cycle at this site. Though photosynthesis could start earlier, the minimum temperature for cambial activity is at 5-6 ^{o}C (Fatichi et al., 2014) and normally occurs from May at this elevation. Xylogenesis monitoring around 2000 m a.s.l. indicates that xylogenesis of *Picea abies* started around the end of May (Rossi et al., 2006).

Remarkably, no relationship was observed when the temperature of the previous year was correlated with the GPP of the current year. This points to the unique and complex growth process at the study site and agrees with the findings of Cabon et al. (2022) that gymnosperm relies more on the current year's carbon uptake and less on the previous year than angiosperms. In addition, the correlation with precipitation of the current year did not yield any coherent result. However, the December precipitation of the previous year showed a link with the May GPP. The lack of correlation with current year precipitation suggests that precipitation during the spring and summer is not a limiting factor (Fatichi et al., 2014; Roebroek et al., 2020), while the December precipitation, which is normally in the form of snow, could be attributed to the snow effect – where snow makes water available for plant uptake and biochemical processes, particularly in the early part of season (Zeeman et al., 2017).

4.3 Relationship between GPP and xylem anatomy

In the analysis of the EC dataset, we observed that the daytime method and constant USTAR threshold showed a better correlation with the anatomical series than the night-time method. The result of the daytime time method using a constant USTAR threshold showed a mixture of positive and marginally significant connections between the EC monthly GPP with NUM_EW and NUM_LW. Only the correlation between the NUM_LW and the October GPP was positively significant. The CWA_EW and CWA_LW showed an overall negative relation with the EC GPP. This is contrary to the result obtained by Puchi et al. (Unpublished Manuscript) at a *Pinus strobus* site in Ontario, Canada, where strong positive correlations between xylem anatomical proxies of biomass and summer GPP were observed. Two major reasons could be identified. Firstly, the functionality of EC towers in the Alps considers two terms of mass conservation, the vertical turbulent flux, and the storage flux thereby neglecting advection and horizontal turbulent flux. Consequently, most of the carbon absorbed or stored by forested ecosystems in the Alps is not accounted for due to the absence of a reliable technique to measure advective fluxes on a sloping terrain (Montagnani et al., 2009). Secondly, the carbon assimilated during photosynthesis could have been allocated to other pools such as non-structural carbohydrates (NSC) or utilized to build below-ground biomass (Cabon et al., 2022; Delpierre et al., 2016; Dixon et al., 1994; Richardson et al., 2013). The latter is particularly relevant in our study site at 1735 m a.s.l., as it has been shown that NSC increases with an increase in elevation (Wieser et al., 2019). More so, trees under stress tend to accumulate NSC (Fatichi et al., 2014; Rocha et al., 2006). Though at this elevation, *Picea abies* is at its optimal condition (Castagneri et al., 2017), we observed in one of the trees frost-damaged xylem cells (1951) and in another, wavy rings (early 1980s). Probably, NSC increased in such suboptimal conditions. This calls for integrated measurement of other carbon storage sources for a definitive conclusion and to ensure closure in forest carbon balance.

Also, as a mature and closed-canopy forest, nutrient limitations and environmental factors could have caused the decoupling between the EC GPP and the xylem anatomical proxies of biomass. Studies have shown that cambial activity is characteristically more sensitive than carbon uptake to prevailing environmental conditions, such as temperature, water and nutrient availability (Cabon et al., 2020; Fatichi et al., 2014; Peters et al., 2021). Furthermore, studying the anatomical proxies of biomass at intra-annual resolution hypothetically provides a better view of the GPP-biomass relationship. Our result concurs with the fact that C assimilation (source-limited) and tree growth (sink-limited) are essentially separate and controlled by different biophysical processes (Cabon et al., 2022; Fatichi et al., 2014), hence the absence of

positive relationship between GPP and tree biomass increment. Even between the studied anatomical proxies of biomass, CWA and NUM, they are controlled by different physiological processes (Rossi et al., 2006) and as such would relate to GPP differently. This understanding necessitated the separate study of these anatomical traits rather than merely measuring the tree rings width.

On a positive note, we recorded marginal positive correlation for NUM_EW and NUM_LW with GPP, especially from summer to autumn. This showed that long and warm growing season, with temperature above 5^{o}C until autumn, benefit GPP and finally biomass production (NUM_EW and NUM_LW).

Conclusively, since there was no evident association between the CWA_EW, CWA_LW, NUM_EW, and NUM_LW (measures of EW and LW biomass) with the spring_GPP and summer_GPP respectively, then the initial hypothesis of direct influence of GPP to woody biomass production at our study site is rejected. Rather, the alternative hypothesis which states that most carbon taken during photosynthesis is not rapidly mobilized for cell growth, is validated and thus did not improve the link between EC flux dataset with tree-ring information. Also, based on clear understanding of the complex climate-carbon uptake-tree biomass relationships, the climatic influence on carbon flux and tree biomass proxies are mutually exclusive and therefore, our second hypothesis is rejected.

5. CONCLUSION

The quantification of carbon balance in the forest ecosystem using eddy covariance techniques has been besieged with some technicalities and uncertainties. On the one hand, there was need to link outcomes from EC with other forest productivity measurements to ensure that the fate of carbon and the role of the forest ecosystem in the face of the rising incidence of climate change is empirically predictable. On the other hand, efforts to connect EC techniques data with other methods have resulted in a mixture of conclusions where some concurred with EC data and others did not.

This thesis for the first time used xylem anatomical traits, based on dendroanatomy, to study the complex relationships between forest carbon fluxes (as recorded by EC) with the intra-annual variabilities of woody biomass inferred from xylem anatomical series.

In a complementary and hypothetical state, the xylem anatomical features, as proxies for forest productivity, would be correspondent and harmonious with the EC carbon fluxes, in this sense, the GPP. Similarly, if some of the photosynthates are promptly utilized for cell growth, it is expected that xylem earlywood biomass would correlate with spring GPP and the xylem latewood biomass with the late summer GPP.

The result of the study demonstrated that the xylem earlywood and latewood biomass are incongruous with EC GPP at Renon forest likely because most of the photosynthates are not rapidly mobilized for cell growth.

On the positive side, it was observed that GPP increases with a lengthy growing season and also that xylem earlywood biomass responded favourably to winter precipitation while xylem latewood biomass was influenced more by temperatures. This indicates that wood anatomy can improve our understanding of the complex climate-carbon uptake-biomass growth relationships compared to classical approaches.

Finally, to achieve a compatible result between EC fluxes and tree-ring information, further research should be carried out in European forests with EC towers on level terrain. More so, concerted efforts should be made to eliminate sources of doubt and flux omission from the flux towers. The tree rings as an archive of environmental and physiological imprints are better positioned to reveal the true carbon balance in the forest and data from dendroanatomy should be widely used as the proxy for forest productivity measures.

References

Alexander, M.R., Rollinson, C.R., Babst, F., Trouet, V., Moore, D.J.P., 2018. Relative influences of multiple sources of uncertainty on cumulative and incremental tree-ring-derived aboveground biomass estimates. Trees 32, 265–276. https://doi.org/10.1007/s00468-017-1629-0

Anić, M., Ostrogović Sever, M., Alberti, G., Balenović, I., Paladinić, E., Peressotti, A., Tijan, G., Večenaj, Ž., Vuletić, D., Marjanović, H., 2018. Eddy Covariance vs. Biometric Based Estimates of Net Primary Productivity of Pedunculate Oak (Quercus robur L.) Forest in Croatia during Ten Years. Forests 9, 764. https://doi.org/10.3390/f9120764

Aubinet, M., Hurdebise, Q., Chopin, H., Debacq, A., De Ligne, A., Heinesch, B., Manise, T., Vincke, C., 2018. Inter-annual variability of Net Ecosystem Productivity for a temperate mixed forest: A predominance of carry-over effects? Agric. For. Meteorol. 262, 340–353. https://doi.org/10.1016/j.agrformet.2018.07.024

Babst, F., Alexander, M.R., Szejner, P., Bouriaud, O., Klesse, S., Roden, J., Ciais, P., Poulter, B., Frank, D., Moore, D.J.P., Trouet, V., 2014a. A tree-ring perspective on the terrestrial carbon cycle. Oecologia 176, 307–322. https://doi.org/10.1007/s00442-014-3031-6

Babst, F., Bodesheim, P., Charney, N., Friend, A.D., Girardin, M.P., Klesse, S., Moore, D.J.P., Seftigen, K., Björklund, J., Bouriaud, O., Dawson, A., DeRose, R.J., Dietze, M.C., Eckes, A.H., Enquist, B., Frank, D.C., Mahecha, M.D., Poulter, B., Record, S., Trouet, V., Turton, R.H., Zhang, Z., Evans, M.E.K., 2018. When tree rings go global: Challenges and opportunities for retro- and prospective insight. Quat. Sci. Rev. 197, 1–20. https://doi.org/10.1016/j.quascirev.2018.07.009

Babst, F., Bouriaud, O., Papale, D., Gielen, B., Janssens, I.A., Nikinmaa, E., Ibrom, A., Wu, J., Bernhofer, C., Köstner, B., Grünwald, T., Seufert, G., Ciais, P., Frank, D., 2014b. Above-ground woody carbon sequestration measured from tree rings is coherent with net ecosystem productivity at five eddy-covariance sites. New Phytol. 201, 1289–1303. https://doi.org/10.1111/nph.12589

Babst, F., Poulter, B., Trouet, V., Tan, K., Neuwirth, B., Wilson, R., Carrer, M., Grabner, M., Tegel, W., Levanic, T., Panayotov, M., Urbinati, C., Bouriaud, O., Ciais, P., Frank, D., 2013. Site- and species-specific responses of forest growth to climate across the European continent. Glob. Ecol. Biogeogr. 22, 706–717. https://doi.org/10.1111/geb.12023

Baldocchi, D., Chu, H., Reichstein, M., 2018. Inter-annual variability of net and gross ecosystem carbon fluxes: A review. Agric. For. Meteorol. 249, 520–533. https://doi.org/10.1016/j.agrformet.2017.05.015

Baldocchi, D.D., 2003. Assessing the eddy covariance technique for evaluating carbon dioxide exchange rates of ecosystems: past, present and future. Glob. Change Biol. 9, 479–492. https://doi.org/10.1046/j.1365-2486.2003.00629.x

Berger, T.W., Köllensperger, G., Wimmer, R., 2004. Plant-soil feedback in spruce (Picea abies) and mixed spruce-beech (Fagus sylvatica) stands as indicated by dendrochemistry. Plant Soil 264, 69–83. https://doi.org/10.1023/B:PLSO.0000047714.43253.25

Björklund, J., Seftigen, K., Schweingruber, F., Fonti, P., von Arx, G., Bryukhanova, M.V., Cuny, H.E., Carrer, M., Castagneri, D., Frank, D.C., 2017. Cell size and wall dimensions drive distinct variability of earlywood and latewood density in Northern Hemisphere conifers. New Phytol. 216, 728–740. https://doi.org/10.1111/nph.14639

Bunn, A.G., 2008. A dendrochronology program library in R (dplR). Dendrochronologia 26, 115–124. https://doi.org/10.1016/j.dendro.2008.01.002

Cabon, A., Kannenberg, S.A., Arain, A., Babst, F., Baldocchi, D., Belmecheri, S., Delpierre, N., Guerrieri, R., Maxwell, J.T., McKenzie, S., Meinzer, F.C., Moore, D.J.P., Pappas, C., Rocha, A.V., Szejner, P., Ueyama, M., Ulrich, D., Vincke, C., Voelker, S.L., Wei, J., Woodruff, D., Anderegg, W.R.L., 2022. Cross-biome synthesis of source versus sink limits to tree growth. Science 376, 758–761. https://doi.org/10.1126/science.abm4875

Cabon, A., Peters, R.L., Fonti, P., Martínez-Vilalta, J., De Cáceres, M., 2020. Temperature and water potential co-limit stem cambial activity along a steep elevational gradient. New Phytol. 226, 1325–1340. https://doi.org/10.1111/nph.16456

Campbell, R., McCarroll, D., Loader, N.J., Grudd, H., Robertson, I., Jalkanen, R., 2007. Blue intensity in Pinus sylvestris tree-rings: developing a new palaeoclimate proxy. The Holocene 17, 821–828. https://doi.org/10.1177/0959683607080523

Carrer, M., von Arx, G., Castagneri, D., Petit, G., 2015. Distilling allometric and environmental information from time series of conduit size: the standardization issue and its relationship to tree hydraulic architecture. Tree Physiol. 35, 27–33. https://doi.org/10.1093/treephys/tpu108

Castagneri, D., Fonti, P., von Arx, G., Carrer, M., 2017. How does climate influence xylem morphogenesis over the growing season? Insights from long-term intra-ring anatomy in *Picea abies*. Ann. Bot. mcw274. https://doi.org/10.1093/aob/mcw274

Cook, E., Kairiūkštis, L. (Eds.), 1990. Methods of dendrochronology: applications in the environmental science. Kluwer Academic Publishers ; International Institute for Applied Systems Analysis, Dordrecht, Netherlands ; Boston : [S.l.].

Cornes, R.C., van der Schrier, G., van den Besselaar, E.J.M., Jones, P.D., 2018. An Ensemble Version of the E-OBS Temperature and Precipitation Data Sets. J. Geophys. Res. Atmospheres 123, 9391–9409. https://doi.org/10.1029/2017JD028200

Crabbe, R.A., Dash, J., Rodriguez-Galiano, V.F., Janous, D., Pavelka, M., Marek, M.V., 2016. Extreme warm temperatures alter forest phenology and productivity in Europe. Sci. Total Environ. 10.

Cuny, H.E., Rathgeber, C.B.K., Frank, D., Fonti, P., Mäkinen, H., Prislan, P., Rossi, S., del Castillo, E.M., Campelo, F., Vavrčík, H., Camarero, J.J., Bryukhanova, M.V., Jyske, T., Gričar, J., Gryc, V., De Luis, M., Vieira, J., Čufar, K., Kirdyanov, A.V., Oberhuber, W., Treml, V., Huang, J.-G., Li, X., Swidrak, I., Deslauriers, A., Liang, E., Nöjd, P., Gruber, A., Nabais, C., Morin, H., Krause, C., King, G., Fournier, M., 2015. Woody biomass production lags stem-girth increase by over one month in coniferous forests. Nat. Plants 1, 15160. https://doi.org/10.1038/nplants.2015.160

Delpierre, N., Berveiller, D., Granda, E., Dufrêne, E., 2016. Wood phenology, not carbon input, controls the interannual variability of wood growth in a temperate oak forest. New Phytol. 210, 459–470. https://doi.org/10.1111/nph.13771

Dixon, R.K., Brown, S., Houghton, R.A., Solomon, A.M., Trexler, M.C., Wisniewski, J., 1994. Carbon Pools and Flux of Global Forest Ecosystems. Science 263, 185–190.

Fatichi, S., Leuzinger, S., Körner, C., 2014. Moving beyond photosynthesis: from carbon source to sink-driven vegetation modeling. New Phytol. 201, 1086–1095.

Feigenwinter, C., Bernhofer, C., Eichelmann, U., Heinesch, B., Hertel, M., Janous, D., Kolle, O., Lagergren, F., Lindroth, A., Minerbi, S., 2008. Comparison of horizontal and vertical advective CO2 fluxes at three forest sites. Agric. For. Meteorol. 148, 12–24.

Fonti, P., von Arx, G., García-González, I., Eilmann, B., Sass-Klaassen, U., Gärtner, H., Eckstein, D., 2010. Studying global change through investigation of the plastic responses of xylem anatomy in tree rings. New Phytol. 185, 42–53. https://doi.org/10.1111/j.1469-8137.2009.03030.x

Fritts, H., 1976. Tree Rings and Climate. Elsevier. https://doi.org/10.1016/B978-0-12-268450-0.X5001-0
Gobiet, A., Kotlarski, S., Beniston, M., Heinrich, G., Rajczak, J., Stoffel, M., 2014. 21st century climate change in the European Alps—A review. Sci. Total Environ. 493, 1138–1151.
González-García, M., Almeida, A.C., Hevia, A., Majada, J., Beadle, C., 2016. Application of a process-based model for predicting the productivity of Eucalyptus nitens bioenergy plantations in Spain. GCB Bioenergy 8, 194–210. https://doi.org/10.1111/gcbb.12256
Jia, H., Zhou, Y., Zhang, J., Sun, S., Meng, P., 2022. Early–latewood carbon isotope enhances the understanding of the relationship between tree biomass growth and forest-level carbon fluxes. Agric. For. Meteorol. 315, 108818. https://doi.org/10.1016/j.agrformet.2022.108818
Lasslop, G., Reichstein, M., Papale, D., Richardson, A.D., Arneth, A., Barr, A., Stoy, P., Wohlfahrt, G., 2010. Separation of net ecosystem exchange into assimilation and respiration using a light response curve approach: critical issues and global evaluation. Glob. Change Biol. 16, 187–208. https://doi.org/10.1111/j.1365-2486.2009.02041.x
Lempereur, M., Martin-StPaul, N.K., Damesin, C., Joffre, R., Ourcival, J.-M., Rocheteau, A., Rambal, S., 2015. Growth duration is a better predictor of stem increment than carbon supply in a Mediterranean oak forest: implications for assessing forest productivity under climate change. New Phytol. 207, 579–590. https://doi.org/10.1111/nph.13400
Liu, Y., Wu, C., Liu, L., Gu, C., Andrew Black, T., Jassal, R.S., Hörtnagl, L., Montagnani, L., Moyano, F., Varlagin, A., Altaf Arain, M., Govind, A., 2021. Interannual and spatial variability of net ecosystem production in forests explained by an integrated physiological indicator in summer. Ecol. Indic. 129, 107982. https://doi.org/10.1016/j.ecolind.2021.107982
Marcolla, B., Cescatti, A., Montagnani, L., Manca, G., Kerschbaumer, G., Minerbi, S., 2005. Importance of advection in the atmospheric CO2 exchanges of an alpine forest. Agric. For. Meteorol. 130, 193–206. https://doi.org/10.1016/j.agrformet.2005.03.006
Martin, A.R., Doraisami, M., Thomas, S.C., 2018. Global patterns in wood carbon concentration across the world's trees and forests. Nat. Geosci. 11, 915–920. https://doi.org/10.1038/s41561-018-0246-x
McKenzie, S.M., Pisaric, M.F.J., Arain, M.A., 2021. Comparison of tree-ring growth and eddy covariance-based ecosystem productivities in three different-aged pine plantation forests. Trees 35, 583–595. https://doi.org/10.1007/s00468-020-02061-z
Montagnani, L., Manca, G., Canepa, E., Georgieva, E., Acosta, M., Feigenwinter, C., Janous, D., Kerschbaumer, G., Lindroth, A., Minach, L., 2009. A new mass conservation approach to the study of CO2 advection in an alpine forest. J. Geophys. Res. Atmospheres 114.
Niu, S., Luo, Y., Fei, S., Montagnani, L., Bohrer, G.I.L., Janssens, I.A., Gielen, B., Rambal, S., Moors, E., Matteucci, G., 2011. Seasonal hysteresis of net ecosystem exchange in response to temperature change: patterns and causes. Glob. Change Biol. 17, 3102–3114.
Pacheco Solana, A., Camarero, J.J., Carrer, M., 2018. Dendroanatomy: a new approach to sharpen the focus on the climatic drivers of tree growth in the Mediterranean. PhD Thesis UNIPD.
Papale, D., Migliavacca, M., Cremonese, E., Cescatti, A., Alberti, G., Balzarolo, M., Belelli Marchesini, L., Canfora, E., Casa, R., Duce, P., Facini, O., Galvagno, M., Genesio, L., Gianelle, D., Magliulo, V., Matteucci, G., Montagnani, L., Petrella, F., Pitacco, A., Seufert, G., Spano, D., Stefani, P., Vaccari, F.P., Valentini, R., 2015. Carbon, Water

and Energy Fluxes of Terrestrial Ecosystems in Italy, in: Valentini, R., Miglietta, F. (Eds.), The Greenhouse Gas Balance of Italy, Environmental Science and Engineering. Springer Berlin Heidelberg, Berlin, Heidelberg, pp. 11–45. https://doi.org/10.1007/978-3-642-32424-6_2

Pappas, C., Maillet, J., Rakowski, S., Baltzer, J.L., Barr, A.G., Black, T.A., Fatichi, S., Laroque, C.P., Matheny, A.M., Roy, A., Sonnentag, O., Zha, T., 2020. Aboveground tree growth is a minor and decoupled fraction of boreal forest carbon input. Agric. For. Meteorol. 290, 108030. https://doi.org/10.1016/j.agrformet.2020.108030

Pastorello, G., 2020. The FLUXNET2015 dataset and the ONEFlux processing pipeline for eddy covariance data 27.

Peng, C., Zhou, X., Zhao, S., Wang, X., Zhu, B., Piao, S., Fang, J., 2009. Quantifying the response of forest carbon balance to future climate change in Northeastern China: Model validation and prediction. Glob. Planet. Change 66, 179–194. https://doi.org/10.1016/j.gloplacha.2008.12.001

Peters, R.L., Steppe, K., Cuny, H.E., De Pauw, D.J.W., Frank, D.C., Schaub, M., Rathgeber, C.B.K., Cabon, A., Fonti, P., 2021. Turgor – a limiting factor for radial growth in mature conifers along an elevational gradient. New Phytol. 229, 213–229. https://doi.org/10.1111/nph.16872

Prendin, A.L., Petit, G., Carrer, M., Fonti, P., Björklund, J., von Arx, G., 2017. New research perspectives from a novel approach to quantify tracheid wall thickness. Tree Physiol. 37, 976–983. https://doi.org/10.1093/treephys/tpx037

Puchi, P.F., Khomik, M., Frigo, D., Arain, M.A., Fonti, P., von Arx, G., Castagneri, D., n.d. Revealing intra-annual carbon sequestration patterns through xylem anatomy and eddy covariance fluxes in eastern white pine. [Unpublished manuscript].

Rannik, Ü., Vesala, T., Peltola, O., Novick, K.A., Aurela, M., Järvi, L., Montagnani, L., Mölder, M., Peichl, M., Pilegaard, K., Mammarella, I., 2020. Impact of coordinate rotation on eddy covariance fluxes at complex sites. Agric. For. Meteorol. 287, 107940. https://doi.org/10.1016/j.agrformet.2020.107940

Reichstein, M., Falge, E., Baldocchi, D., Papale, D., Aubinet, M., Berbigier, P., Bernhofer, C., Buchmann, N., Gilmanov, T., Granier, A., Grünwald, T., Havránková, K., Ilvesniemi, H., Janous, D., Knohl, A., Laurila, T., Lohila, A., Loustau, D., Matteucci, G., Meyers, T., Miglietta, F., Ourcival, J.-M., Pumpanen, J., Rambal, S., Rotenberg, E., Sanz, M., Tenhunen, J., Seufert, G., Vaccari, F., Vesala, T., Yakir, D., Valentini, R., 2005. On the separation of net ecosystem exchange into assimilation and ecosystem respiration: review and improved algorithm. Glob. Change Biol. 11, 1424–1439. https://doi.org/10.1111/j.1365-2486.2005.001002.x

Richardson, A.D., Carbone, M.S., Keenan, T.F., Czimczik, C.I., Hollinger, D.Y., Murakami, P., Schaberg, P.G., Xu, X., 2013. Seasonal dynamics and age of stemwood nonstructural carbohydrates in temperate forest trees. New Phytol. 197, 850–861.

Rocha, A.V., Goulden, M.L., Dunn, A.L., Wofsy, S.C., 2006. On linking interannual tree ring variability with observations of whole-forest CO2 flux. Glob. Change Biol. 12, 1378–1389. https://doi.org/10.1111/j.1365-2486.2006.01179.x

Roebroek, C.T.J., Melsen, L.A., Hoek van Dijke, A.J., Fan, Y., Teuling, A.J., 2020. Global distribution of hydrologic controls on forest growth. Hydrol. Earth Syst. Sci. 24, 4625–4639. https://doi.org/10.5194/hess-24-4625-2020

Rossi, S., Deslauriers, A., Anfodillo, T., 2006. Assessment of Cambial Activity and Xylogenesis by Microsampling Tree Species: An Example at the Alpine Timberline. IAWA J. 27, 383–394. https://doi.org/10.1163/22941932-90000161

Seyednasrollah, B., Bowling, D.R., Cheng, R., Logan, B.A., Magney, T.S., Frankenberg, C., Yang, J.C., Young, A.M., Hufkens, K., Arain, M.A., Black, T.A., Blanken, P.D.,

Bracho, R., Jassal, R., Hollinger, D.Y., Law, B.E., Nesic, Z., Richardson, A.D., 2021. Seasonal variation in the canopy color of temperate evergreen conifer forests. New Phytol. 229, 2586–2600. https://doi.org/10.1111/nph.17046

Sha, Z., Bai, Y., Li, R., Lan, H., Zhang, X., Li, J., Liu, X., Chang, S., Xie, Y., 2022. The global carbon sink potential of terrestrial vegetation can be increased substantially by optimal land management. Commun. Earth Environ. 3, 8. https://doi.org/10.1038/s43247-021-00333-1

Teets, A., Fraver, S., Hollinger, D.Y., Weiskittel, A.R., Seymour, R.S., Richardson, A.D., 2018. Linking annual tree growth with eddy-flux measures of net ecosystem productivity across twenty years of observation in a mixed conifer forest. Agric. For. Meteorol. 249, 479–487. https://doi.org/10.1016/j.agrformet.2017.08.007

Tramontana, G., Migliavacca, M., Jung, M., Reichstein, M., Keenan, T.F., Camps-Valls, G., Ogee, J., Verrelst, J., Papale, D., 2020. Partitioning net carbon dioxide fluxes into photosynthesis and respiration using neural networks. Glob. Change Biol. 26, 5235–5253. https://doi.org/10.1111/gcb.15203

von Arx, G., Carrer, M., 2014. ROXAS – A new tool to build centuries-long tracheid-lumen chronologies in conifers. Dendrochronologia 32, 290–293. https://doi.org/10.1016/j.dendro.2013.12.001

von Arx, G., Crivellaro, A., Prendin, A.L., Čufar, K., Carrer, M., 2016. Quantitative Wood Anatomy—Practical Guidelines. Front. Plant Sci. 7. https://doi.org/10.3389/fpls.2016.00781

Wehr, R., Munger, J.W., McManus, J.B., Nelson, D.D., Zahniser, M.S., Davidson, E.A., Wofsy, S.C., Saleska, S.R., 2016. Seasonality of temperate forest photosynthesis and daytime respiration. Nature 534, 680–683. https://doi.org/10.1038/nature17966

Wieser, G., Oberhuber, W., Gruber, A., 2019. Effects of Climate Change at Treeline: Lessons from Space-for-Time Studies, Manipulative Experiments, and Long-Term Observational Records in the Central Austrian Alps. Forests 10, 508. https://doi.org/10.3390/f10060508

Xu, K., Wang, X., Liang, P., Wu, Y., An, H., Sun, H., Wu, P., Wu, X., Li, Q., Guo, X., Wen, X., Han, W., Liu, C., Fan, D., 2019. A new tree-ring sampling method to estimate forest productivity and its temporal variation accurately in natural forests. For. Ecol. Manag. 433, 217–227. https://doi.org/10.1016/j.foreco.2018.10.066

Zanotelli, D., Montagnani, L., Manca, G., Scandellari, F., Tagliavini, M., 2015. Net ecosystem carbon balance of an apple orchard. Eur. J. Agron. 63, 97–104. https://doi.org/10.1016/j.eja.2014.12.002

Zeeman, M.J., Mauder, M., Steinbrecher, R., Heidbach, K., Eckart, E., Schmid, H.P., 2017. Reduced snow cover affects productivity of upland temperate grasslands. Agric. For. Meteorol. 232, 514–526.

Zweifel, R., Eugster, W., Etzold, S., Dobbertin, M., Buchmann, N., Häsler, R., 2010. Link between continuous stem radius changes and net ecosystem productivity of a subalpine Norway spruce forest in the Swiss Alps. New Phytol. 187, 819–830. https://doi.org/10.1111/j.1469-8137.2010.03301.x

Annexes

Annex 1: The correlation between previous year temperature and GPP of the current year.

		GPP current year											
Prev. Yr		JAN	FEB	MAR	APR	MAY	JUN	JUL	AUG	SEP	OCT	NOV	DEC
T	Jan	0.25549775	0.3776703	0.26575624	0.00328436	-0.0323052	0.23091893	0.23647575	0.13312617	0.2934771	0.17555258	0.45115557	0.34083014
e	Feb	-0.0794086	-0.0285378	0.03032547	-0.2349584	-0.2651909	-0.3216314	0.02443445	-0.4255802	-0.4097147	-0.1881518	-0.3552466	-0.5635982
m	Mar	0.20711537	0.17148379	0.07883873	-0.36476	-0.2755218	0.00994993	-0.0361595	-0.146147	-0.1372133	0.03533153	-0.2569136	-0.1347735
p	Apr	0.07430152	0.25141993	0.19256278	0.19516771	0.14796881	0.2088659	0.56549546	0.21295499	0.3236901	0.52792186	0.42655309	0.05153722
e	May	-0.1725136	-0.0612398	-0.2054006	-0.4319363	-0.3374675	0.12736191	0.10828689	0.37003519	0.15665799	0.27357605	0.00554416	0.14762402
r	Jun	-0.1794385	-0.2651687	-0.4367108	-0.0289844	0.05317131	-0.1008664	-0.1120858	-0.0382652	-0.2340934	-0.1069943	-0.3812054	-0.315962
a	Jul	-0.1150716	-0.1904111	-0.1180067	0.40492402	0.29916241	0.04410984	0.01024938	0.05250086	-0.0375327	-0.0262511	0.07789751	0.11411421
t	Aug	-0.3703081	-0.3518265	-0.2614853	-0.3114479	0.03346236	0.0989267	0.04591637	0.33430463	0.15885027	0.32427175	-0.0616281	-0.065857
u	Sep	0.17318935	0.13544774	0.15782674	0.4696354	0.31794564	0.21071574	0.00265408	0.04723167	0.12397361	0.0766143	0.19723278	0.23542265
r	Oct	0.15713103	0.09512351	0.26453098	0.24485733	-0.0534278	-0.0210124	-0.2185746	-0.1920719	-0.1045647	-0.1756771	-0.4005888	0.15656302
e	Nov	0.26891854	0.24851948	0.29780047	0.60770352	0.35369492	0.52520336	0.2969728	0.38344156	0.23175672	0.29512635	0.12908465	0.0985169
	Dec	0.14329029	0.06858507	0.1945447	0.35036875	0.0163473	-0.0325087	0.05099964	-0.0217651	0.03858481	0.14237181	0.10657313	0.00888452

Annex 2: variabilities between monthly temperature (current year) and anatomical series.

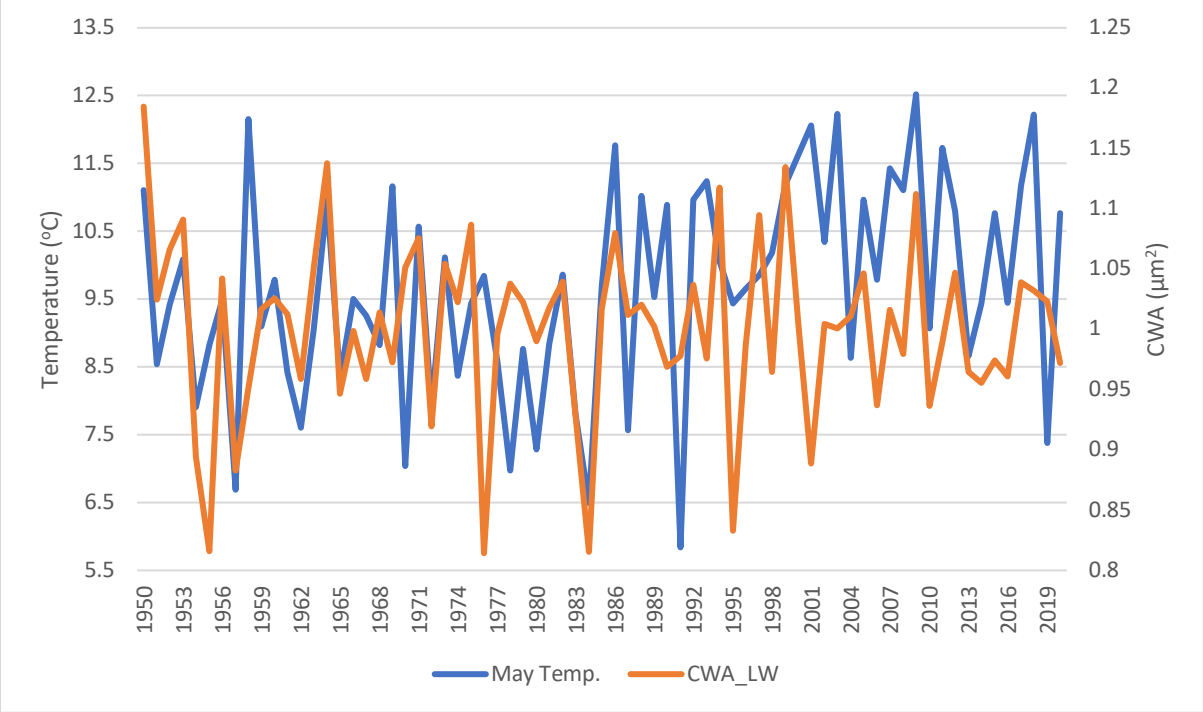

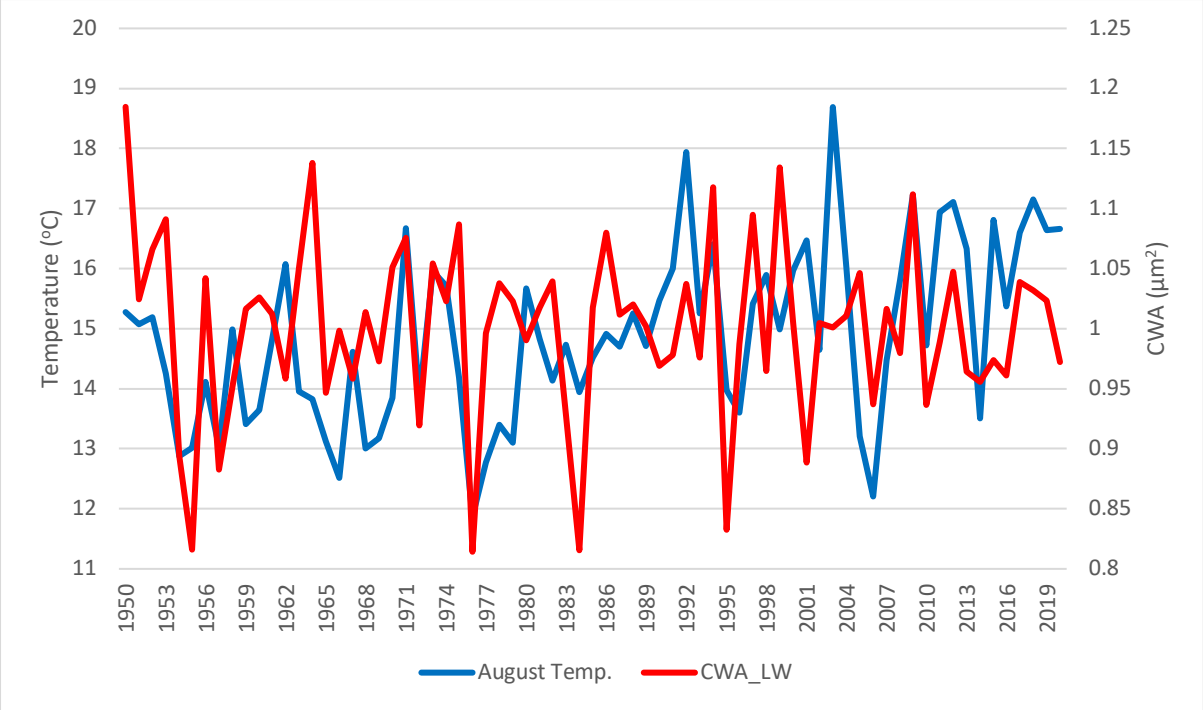
Temperature (°C)
CWA (µm²)
August Temp.
CWA_LW

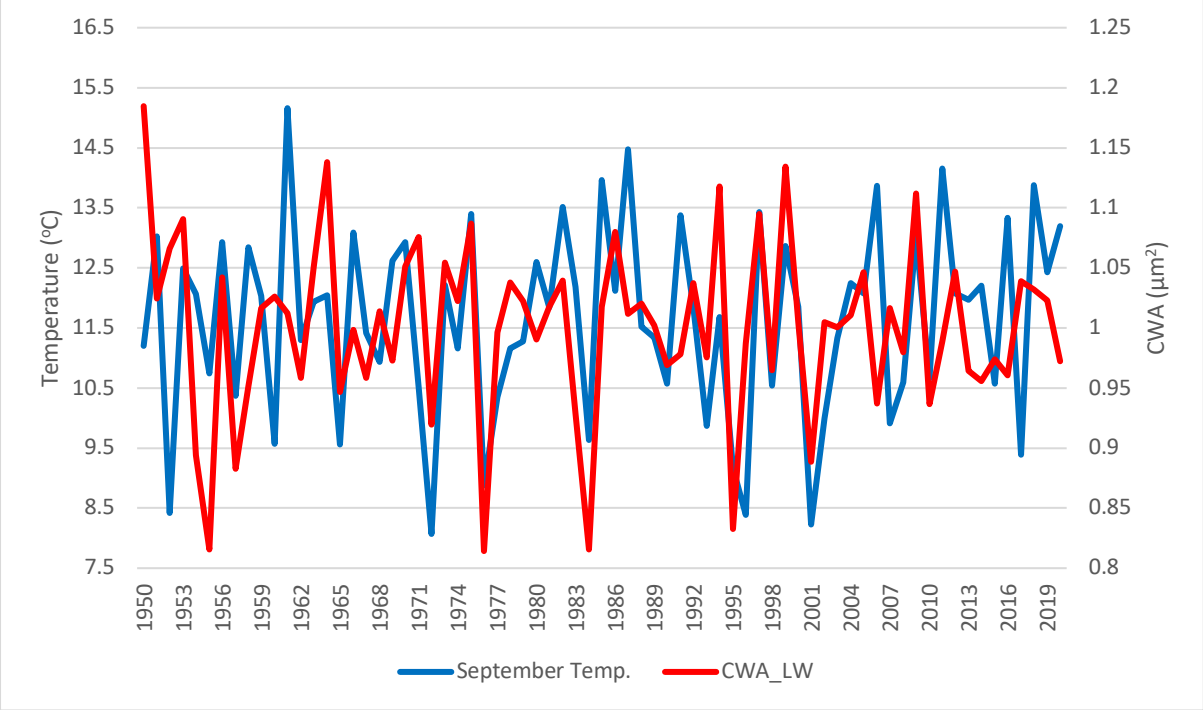
Temperature (°C)
CWA (µm²)
September Temp.
CWA_LW